https://doi.org/10.5194/egusphere-2026-4244
Preprint. Discussion started: 31 July 2026

Measurement report: Unravelling the Mechanisms and Chemical Drivers of New Particle Formation in Chennai, a Tropical Coastal Megacity in India Influenced by an Urban Forest

Mangattayil Devaprasad[1,2,*,#], Amrutha M. Sathyan[1,2,#], Tanmay Kishor Joshi[1,2], Supriya Dey[1,2], Geethanjali Rajendran Malavika[1,2], Yougal Sapkota[2,3], Rizana Salim[1,2], Shailina Srivastava[1,2], Insha Amin[1,2], Govindan Pandithurai[2], Ravikrishna Raghunathan[2,3], Pengfei Liu[4], and Sachin S. Gunthe[1,2,*]

[1]Environmental Engineering Division, Department of Civil Engineering, Indian Institute of Technology Madras, Chennai, India

[2]Center for Atmospheric and Climate Sciences, Indian Institute of Technology Madras, Chennai, India

[3]Department of Chemical Engineering, Indian Institute of Technology Madras, Chennai, India

[4]School of Earth and Atmospheric Sciences, Georgia Institute of Technology, Atlanta, GA, USA

Keywords: New particle formation, Particle growth, Coastal urban atmosphere, Volatile organic compounds, Atmospheric aerosols, Source apportionment, Positive matrix factorization

[#]These authors contributed equally to this work.

*_Correspondence to:_ Mangattayil Devaprasad (devaprasad@cacs.iitm.ac.in) and Sachin S. Gunthe (s.gunthe@iitm.ac.in).

https://doi.org/10.5194/egusphere-2026-4244
Preprint. Discussion started: 31 July 2026

Abstract

Chemically resolved gas- and particle-phase measurements capable of constraining new particle formation (NPF) remain scarce in South Asia. Here, we investigate the precursors driving NPF in a coastal megacity and examine why only a subset of nucleation events evolves into sustained particle growth. We present the first comprehensive 20-day field study in a Bay of Bengal coastal megacity, integrating aerosol microphysical, chemical, gas-phase, and VOC measurements with positive matrix factorization (PMF). Photochemically driven formation of 10-30 nm particles occurred between 07:00 and 11:00 IST, whereas sustained growth into the accumulation mode occurred only 2 of 20 days, with growth rates of 4.53 and 3.43 nm h^{-1}. The particle formation rate, condensation sink (CS), and coagulation sink did not differ between growth and non-growth days, indicating that neither formation intensity nor scavenging distinguished the two regimes. Instead, sustained growth occurred when northerly continental air masses prevailed, whereas growth ceased when a strong sea breeze shifted transport to marine air influenced by power-plant emissions. PMF resolved six factors, including an NPF factor dominated by 10–30 nm particles that was associated with biogenic VOCs. Its invariance between weekdays and weekends, and negative correlation with vehicular traffic factor, indicates that NPF was driven primarily by photo-oxidation of biogenic precursors, rather than by anthropogenic activity. These findings suggest that, in coastal cities, precursor availability and air-mass origin may exert a stronger influence on particle growth than CS, although long-term observations are needed to establish its broader applicability.

https://doi.org/10.5194/egusphere-2026-4244
Preprint. Discussion started: 31 July 2026

1 Introduction

Atmospheric new particle formation (NPF), the process by which low-volatility vapours undergo gas-to-particle conversion to form stable molecular clusters that subsequently grow to detectable sizes, is the single largest source of aerosol particle number in the Earth's troposphere (Kulmala, 2025; Kulmala et al., 2004; Lee et al., 2019; Pöschl, 2005). Globally, NPF is estimated to contribute 45–85 % of present-day cloud condensation nuclei (CCN), thereby exerting a substantial influence on cloud microphysical properties, planetary albedo, and the indirect radiative forcing of climate (Gordon et al., 2017; Merikanto et al., 2009; Sun et al., 2024). NPF is also the dominant source of ultrafine particles (UFP; $d_p < 100$ nm) in many environments, making it an important determinant of human exposure to particles that have been linked to adverse cardiovascular and respiratory health outcomes (Ibald-Mulli et al., 2002; Schraufnagel, 2020).

The mechanistic understanding of atmospheric NPF has advanced considerably over the past decade. In many continental environments, nucleation is initiated by sulfuric acid (H_2SO_4) molecules stabilized by ammonia (NH_3) and amines (Kirkby et al., 2011; Kürten et al., 2014). Highly oxygenated organic molecules (HOMs), formed through the oxidation of biogenic and anthropogenic VOCs, contribute both to nucleation and to the early condensational growth of newly formed clusters (Bianchi et al., 2019; Tiszenkel et al., 2025; Tröstl et al., 2016). Whether these clusters survive and grow to CCN-relevant sizes depends on the balance between supply of condensable precursor vapours and their loss to pre-existing particles through the condensation sink (CS). This evolution is governed by multiple interacting factors, including precursor gas availability, meteorological conditions, atmospheric dynamics, photochemical activity, relative humidity, temperature, and the chemical composition and loading of pre-existing aerosols (Dal Maso et al., 2005; Kanawade et al., 2022; Kulmala et al., 2004).

Despite the high CS characteristic of polluted urban environments, NPF has been widely documented in megacities including Beijing (Chu et al., 2019; Shang et al., 2023; Tang et al., 2025), São Paulo (Backman et al., 2012), Delhi (Ali et al., 2025; Mishra et al., 2023) and Hyderabad (Kanawade et al., 2014b; Sebastian et al., 2022). These observations indicate that sufficiently high production rates of condensable vapours can offset the newly formed clusters and sustain particle formation even under

https://doi.org/10.5194/egusphere-2026-4244
Preprint. Discussion started: 31 July 2026

conditions of an elevated CS. The balance between precursor supply and condensational loss is further modulated by precursor concentrations, and boundary layer dynamics (Du et al., 2022; Kulmala et al., 2017). This interplay becomes particularly complex in coastal urban environments influenced by nearby biogenic emissions, where biogenic and marine sources enhance the supply of condensable vapours that promote nucleation and secondary organic aerosol (SOA) growth, while anthropogenic aerosol loading simultaneously increases the CS, thereby regulating the survival and subsequent growth of newly formed particles (O'Dowd et al., 2002).

Within this global context, observations from India remain surprisingly sparse despite the country's rapid urbanization, diverse climatic regimes, and exceptionally high ambient aerosol loadings. The first evidence of NPF over the Indian subcontinent was reported only in 2005, from New Delhi (Mönkkönen et al., 2005), and by the time of the most recent comprehensive review, only 22 independent field studies had been conducted across the region (Kanawade et al., 2022). Subsequent observations at urban sites including Kanpur and Hyderabad (Kanawade et al., 2014b), the semi-rural site of Gadanki (Kanawade et al., 2014a), Himalayan background locations (Komppula et al., 2009; Singh et al., 2025b), and a six-site synthesis (Sebastian et al., 2022) collectively demonstrate that NPF is widespread during the pre-monsoon season (March–May) across diverse Indian environments, with particle growth rates ranging from 0.2 to 17 nm h^{-1} and particle formation rates spanning three orders of magnitude. Measurements of sub-3 nm clusters at an urban site (Sebastian et al., 2021) have provided rare insights into the earliest stages of particle formation, while observations during the COVID-19 lockdown in Hyderabad offered direct evidence of the nonlinear response of NPF to changes in the balance between precursor supply and the CS. More recently, observations in the Indo-Gangetic plain have examined the combined physical and chemical controls on NPF in megacity Delhi (Ali et al., 2025). Nevertheless, important knowledge gaps remain. First, simultaneous chemically speciated measurements of the gas-phase precursors driving NPF are almost entirely absent at Indian sites (Kanawade et al., 2022). Second, existing observations are heavily concentrated in northern and central India, whereas the tropical coastal regions of the peninsula remain largely unexplored. NPF has been documented at only a few coastal

https://doi.org/10.5194/egusphere-2026-4244
Preprint. Discussion started: 31 July 2026

locations, and almost exclusively under the atypical emission conditions associated with the COVID-19 lockdown.

At this coastal megacity, the most comprehensive chemically and microphysically resolved observations of NPF to date were obtained during the COVID-19 lockdown in 2020. By comparing the lockdown with the subsequent reopening period, Singh et al. (2025a) reported a five- to six-fold increase in NPF event frequency and an 80–250 % increase in CCN concentrations as air masses shifted from marine to continental flow. Based on bulk submicron composition, they further inferred that secondary organic matter, largely of anthropogenic origin, dominated particle growth to CCN-relevant sizes. In a complementary case study, Singh et al. (2023) attributed a single rapid-growth event to sulfate formed from emissions of a coal-fired power-plant located approximately 200 km to the south. Together, these studies established that NPF and subsequent growth to climatically relevant sizes occur at this site and are strongly influenced by air-mass origin. However, they provided only limited insight into the underlying mechanism. Both investigations were conducted under the atypical emission conditions of the COVID-19 lockdown rather than under representative atmospheric conditions, neither included measurements of the gas-phase precursors driving NPF and both relied on bulk submicron composition, which is insensitive to particles smaller than approximately 50 nm and could not resolve the contributing precursor sources. Consequently, the identity of the condensable vapours responsible for particle growth, and the relative contributions of adjacent biogenic emissions and anthropogenic sources remained unresolved, particularly because continental airmasses transported both precursor classes simultaneously. To address these knowledge gaps, we conducted an intensive 20-day field campaign (26 May–14 June 2025) under representative, non-lockdown conditions at the Indian Institute of Technology (IIT) Madras, located along the Bay of Bengal coastal interface. A comprehensive suite of instruments, including a Scanning Mobility Particle Sizer (SMPS), Quadrupole Aerosol Chemical Speciation Monitor (Q-ACSM), Aethalometer, Proton-Transfer-Reaction Time-of-Flight Mass Spectrometer (PTR-TOF-MS), trace-gas analyzers, and an automated weather station, was deployed. Combined with Positive Matrix Factorization (PMF) analysis, these measurements provide the first NPF dataset from southern India that simultaneously couples speciated gas-phase precursors with

https://doi.org/10.5194/egusphere-2026-4244
Preprint. Discussion started: 31 July 2026

submicron aerosol composition and source-resolved contributions. This integrated observational record enables investigation of the mechanisms driving NPF, rather than merely describing its occurrence.

Building on the CS limitation framework proposed for polluted environments (Kulmala et al., 2017), this study examines the processes controlling NPF and subsequent particle growth in a tropical coastal megacity influenced by both anthropogenic emissions and nearby biogenic sources. Using a comprehensive suite of chemical, microphysical, gas-phase, and meteorological measurements collected during the pre-monsoon to the monsoon-onset, we investigate the roles of gas-phase precursor availability, condensation and coagulation sinks, source contributions, and meteorological transport in determining both NPF occurrence and the success of particle growth. Specifically, we address three questions: (i) which precursor sources drive the frequent nucleation events observed at the site; (ii) why only a subset of these events develops into sustained particle growth reaching climatically relevant sizes; and (iii) how mesoscale wind evolution and air-mass origin regulate precursor supply during particle growth. To address these questions, we combine primary-tracer normalized diagnostics, quantitative comparisons of particle formation and scavenging conditions between growth and non-growth events, and PMF source apportionment. This integrated framework enables us to disentangle the coupled influences of precursor availability, particle sinks, and air-mass evolution providing new mechanistic insights into NPF and particle growth in tropical coastal urban environments.

2 Methodology

2.1 Measurement Site and Period

Continuous, high-time-resolution measurements of atmospheric aerosols, trace gases, VOCs, and meteorological parameters were conducted from 26 May to 14 June 2025 at the Indian Institute of Technology Madras (IITM), Chennai, India (12.98° N, 80.22° E; ~10 m above mean sea level). Chennai is one of the largest metropolitan regions in India, with a population of approximately 12.6 million (India Population, 2026). The measurement site is located at the boundary of Guindy National Park (~2.7 km²), a protected tropical urban forest situated immediately to the west of the sampling location

https://doi.org/10.5194/egusphere-2026-4244
Preprint. Discussion started: 31 July 2026

(Fig. S2), providing a configuration suitable for investigating interactions between biogenic emissions from the forest canopy and anthropogenic emissions from the surrounding urban environment.

All instruments were housed in a climate-controlled laboratory on the 5th floor of the Engineering Design Building. Ambient air was sampled through inlet lines positioned approximately 4 m above the rooftop. During the campaign, air masses originated predominantly from the western and northwestern continental sectors, with intermittent marine influence from the southeast (Fig. S2).

2.2 Instrumentation

2.2.1 Particle Number Size Distribution

Particle number size distributions in the diameter range 10–280 nm were measured using a SMPS (TSI Model 3938) consisting of an electrostatic classifier (Model 3082) coupled with a Differential Mobility Analyzer (DMA, Model 3081) and a Condensation Particle Counter (CPC, Model 3772). A Kr-85 neutralizer (Model 3077) was used to establish a bipolar charge distribution. The DMA was operated under negative polarity, and both diffusion and multiple-charge corrections were applied. Sheath and aerosol flow rates were maintained at 10.0 and 1.0 L min^{-1}, respectively (sheath-to-aerosol ratio of 10:1), and the system was operated without an upstream impactor.

2.2.2 Non-refractory submicron aerosol composition

The non-refractory submicron aerosol composition (NR-PM_1) was measured using a Q-ACSM (Aerodyne Research Inc.) at a time resolution of 15 min, with the standard vaporizer maintained at ~600 °C. The instrument was calibrated for ionization efficiency (IE) using ammonium nitrate prior to the campaign. Relative ionization efficiencies (RIEs) were set to 1.4 for organics, 5.24 for NH_4^+, 1.02 for SO_4^{2-}, 1.1 for NO_3^-, and 1.3 for chloride, and the mass calibration factor for nitrate was 7.17×10^{-11}. The composition-dependent collection efficiency was applied during data processing (Middlebrook et al., 2012). Following Ng et al. (2011), 15-min detection limits of 0.40, 0.04, 0.04, 0.33, and 0.03 µg m^{-3} were obtained for organics, sulfate, nitrate, ammonium, and chloride, respectively.

https://doi.org/10.5194/egusphere-2026-4244
Preprint. Discussion started: 31 July 2026

2.2.3 Equivalent black carbon

Equivalent black carbon (eBC) concentrations were measured at 1 min time resolution using a seven-wavelength Aethalometer (AE33; Magee Scientific) operated at a flow rate of 3 L min^{-1}. The instrument applies a dual-spot loading compensation technique to correct for filter loading artefacts (Drinovec et al., 2015). eBC was measured in total suspended particles, as no size-selective inlet (cyclone) was used. Flow calibration was performed prior to the campaign using an external flow calibrator (FlexCal). The wavelength-dependent ratio eBC_{370}/eBC_{880} was used to evaluate the relative contributions of fossil-fuel and biomass-burning sources to the eBC mass loading (Sandradewi et al., 2008).

2.2.4 Trace gases

Trace gases including SO_2 and O_3 were measured using gas analyzers from Thermo Scientific (Models 43i and 49i, respectively). NO_x and NH_3 were measured using a Thermo Scientific Model 17i chemiluminescence analyzer equipped with a high-temperature stainless-steel converter, which sequentially reports NO, NO_2, NO_x, and NH_3. All gas analyzers were zero- and span-calibrated using certified gas standards prior to and during the campaign, and all trace-gas data were averaged to a common 15 min time resolution for subsequent analysis.

2.2.5 Volatile Organic Compounds

Volatile organic compounds (VOCs) were measured using a PTR-TOF-MS 6000 X2 (Ionicon Analytik GmbH, Austria) at 30 s time resolution. Ambient air was sampled through a heated multi-stage Teflon/PEEK inlet (final section held at 80 °C; 1 µm PTFE inline filter replaced weekly) to limit condensation and wall losses. The drift tube was operated at 2.8 mbar, 60 °C, and E/N ≈ 130 Td, with spectra acquired over m/z 21–500. Sensitivities were determined by multipoint calibration against a certified multicomponent VOC standard diluted with VOC-free zero air. Methanol, acetone, isoprene, benzene, toluene, xylenes, and acetonitrile were quantified directly against the standard, whereas monoterpenes, Methyl Vinyl Ketone + Methacrolein (MVK + MACR), and dimethyl sulfide (DMS) were derived from proton-transfer rate constants assuming unit transmission (Cappellin et al., 2012;

https://doi.org/10.5194/egusphere-2026-4244
Preprint. Discussion started: 31 July 2026

Sekimoto et al., 2017). Data were processed in the Ionicon Data Analyzer (IDA v2.2.2.1). Full inlet, ion-chemistry, calibration, and transmission details are given in the Supplement (Sect. S1).

2.2.6 Meteorological Measurements and Reanalysis Data

In situ meteorological parameters like temperature, relative humidity, wind speed, and wind direction were measured at the site using an automated weather station (AWS; Thies Clima, Germany). Boundary layer height (BLH), surface solar radiation downward (SSRD), and total accumulated precipitation, which were not measured in situ, were obtained from the ERA5 reanalysis dataset (Hersbach et al., 2020) at hourly resolution and the nearest grid point to the sampling location.

2.2.7 Air Mass Back-Trajectory Analysis

To identify the regional source and transport pathways of air masses arriving at the receptor, 72-h back trajectories were calculated using the NOAA HYSPLIT model (Stein et al., 2015) at 6-hourly intervals throughout the campaign, with an arrival height of 250 m above ground level over the receptor at 12.98° N, 80.22° E. The model was driven by the GDAS 1° meteorological dataset. Trajectories were used to identify the dominant air-mass source sectors during the campaign. The spatial distribution of total accumulated precipitation underlying the trajectory map (Fig. S3) was obtained from the ERA5 reanalysis.

2.3 Derived NPF parameters

The CS, coagulation sink (CoagS), particle growth rate, apparent formation rate ($J_{10–30}$), and a sulfuric acid proxy concentration (H_2SO_4) were derived from the size-distribution and gas-phase data following established protocols (Dal Maso et al., 2002; Kulmala et al., 2012; Mikkonen et al., 2011; Sun et al., 2024). CS quantifies the loss rate of condensable vapours to the pre-existing aerosol; CoagS the coagulational loss of freshly formed particles to larger particles; growth rate the rate of diameter increase during sustained growth; and $J_{10–30}$ the apparent rate at which particles enter the 10–30 nm window. [H_2SO_4] was estimated from a steady-state proxy, as direct measurements were unavailable. Aerosol acidity was additionally characterised through an ion-balance ratio, the total OH reactivity of the measured species was computed as a precursor-loading metric, and the directional dependence of

https://doi.org/10.5194/egusphere-2026-4244
Preprint. Discussion started: 31 July 2026

all species was examined with pollution wind roses. The full equations, parameter choices, and references for each calculation are given in the Supplement (Sect. S1.2 and S1.3). Time series of $N_{10–30}$, CS, CoagS, and $J_{10–30}$ are shown in Fig. S13, the ion balance in Fig. S5, and the [H_2SO_4] proxy in Fig. S19.

2.4 Source Apportionment Using Positive Matrix Factorization

To identify the species driving NPF, PMF was applied using EPA PMF 5.0 (Norris et al., 2014). PMF decomposes the observed data matrix (***X***) into factor contributions (***G***) and factor profiles (***F***) by minimizing the objective function (*Q*), defined as the sum of squared, uncertainty-weighted residuals (Paatero, 1999; Paatero and Tapper, 1994), as given in Eq. (1).

$$X_{ij} = \sum_{k=1}^{p} g_{ik} f_{kj} + e_{ij} \quad \text{Eq1}$$

The input dataset comprised particle number concentrations in three SMPS size bins ($N_{10–30}$, $N_{30–100}$, $N_{100–280}$), NR-PM_1 chemical components from the Q-ACSM (organics, sulfate, nitrate, ammonium, chloride), eBC, trace gases (NO_x, NH_3, SO_2, O_3), and 10 VOC species from the PTR-TOF-MS (methanol, acetone, isoprene, monoterpenes, MVK + MACR, benzene, toluene, xylenes, DMS, acetonitrile). Similar multi-instrument PMF approaches combining particle, gas-phase, and VOC measurements have previously been applied to investigate atmospheric source contributions and processes (Nursanto et al., 2023; Simon et al., 2025; Zhou et al., 2005). All variables were averaged to a common 15-min time resolution prior to analysis. Particle number concentrations were retained in units of cm^{-3}, whereas ACSM species, eBC, trace gases, and VOCs were expressed in $\mu g\ m^{-3}$. The conversion of trace gases and VOCs from ppb to $\mu g\ m^{-3}$ was performed using the molar volume of an ideal gas calculated from real-time temperature and pressure measured by the automated weather station.

Observation uncertainties were assigned following EPA PMF guidelines (Norris et al., 2014), combining a species-specific relative error fraction with the method detection limit; below-detection, missing, and negative values were handled as detailed in the Supplement (Sect. 1.5). Variables were

https://doi.org/10.5194/egusphere-2026-4244
Preprint. Discussion started: 31 July 2026

classified by their signal-to-noise (S/N) ratio as strong (S/N > 2; included as measured), weak (0.2 < S/N ≤ 2; uncertainties tripled), or bad (S/N ≤ 0.2; excluded).

PMF solutions ranging from three to eight factors were evaluated. The optimal number of factors was selected based on (i) the behavior of Q/Qexp, (ii) physical interpretability of the resolved factor profiles, (iii) scaled-residual distributions, and (iv) minimization of rotational ambiguity. Model robustness was assessed using bootstrap analysis (n = 100) and FPEAK rotational analysis (FPEAK from −1.5 to +1.5). Bootstrap results showed that all factors of the selected solution were reproduced in more than 85 % of runs, indicating high stability, and FPEAK analysis produced minimal variation in Q (<0.4 %), confirming low rotational ambiguity. The selected six-factor solution exhibited stable factor profiles and scaled residuals predominantly within ±3, indicating good model performance. Factor interpretation was based on characteristic tracer species, particle size distributions, and co-variation patterns with gas-phase species. Additional details on PMF input preparation and diagnostics are provided in Section 1.5 of the Supplementary Information.

3 Results and Discussion

3.1 Overview of Aerosol Loading and Meteorological Conditions

The 20-day campaign at IIT Madras spanned the transition from hot, dry pre-monsoon conditions of late May to the onset of the southwest monsoon during the second week of June. HYSPLIT back trajectories indicate that air masses originated predominantly from the western and southern sectors (Fig. S3), consistent with the synoptic scale pre-monsoon circulation over the study site. Mean (± 1 sigma) ambient temperature, relative humidity, and wind speed during the campaign were 31.0 ± 2.6 °C, 79.0 ± 13.1 %, and 2.6 ± 1.1 m s^{-1}, respectively; while the planetary boundary layer height averaged 717 ± 388 m. Surface winds were mainly from west to southwest (Fig. 1, Fig. S4).

3.2 Temporal Variability of Chemical Composition

Time series of NR-PM_1 composition, PNSDs, trace gases, and VOCs (Fig. 1) showed substantial day-to-day variability reflecting changes in air-mass origin, photochemical activity, and local emissions throughout the campaign. The mean NR-PM_1 concentration was 10.66 ± 6.84 µg m^{-3}, substantially

https://doi.org/10.5194/egusphere-2026-4244
Preprint. Discussion started: 31 July 2026

lower than those values reported for northern Indian megacities (Devaprasad et al., 2026b). Organic aerosol dominated the sub-micron mass (6.37 ± 3.64 μg m^{-3}; 60.1 %), followed by sulfate (2.95 ± 3.14 μg m^{-3}; 27.7 %), ammonium (0.90 ± 0.97μg m^{-3}; 9.1 %), nitrate (0.37 ± 0.23 μg m^{-3}; 3.5 %), and chloride (0.06 ± 0.06 μg m^{-3};0.6 %) (Fig. 1b). This organic-rich composition is consistent with substantial SOA production under tropical photochemical conditions. The submicron aerosol remained predominantly acidic throughout the campaign (NH_4^+_meas/NH_4^+_pred < 1; Fig. S5), a condition that influences the partitioning of H_2SO_4 between NPF and condensation onto pre-existing particles (Sipilä et al., 2010). Sulfate exhibited the highest variability of all measured components, with episodic enhancements associated with air masses arriving from the south and southeast that are attributed to the Neyveli thermal power station, located approximately 200 km south of the site (Singh et al., 2023; Fig. S6). In contrast, nitrate and chloride remained consistently low throughout the campaign. Mean equivalent black carbon (eBC) at 880 nm was 1.23 ± 0.55 μg m^{-3}, while the eBC_{370}/eBC_{880} ratio averaged 1.16 ± 0.07 (Fig. S8), indicating that fossil-fuel combustion transported primarily from the west and southwest was the dominant source, with only a minor contribution from biomass-burning (Sandradewi et al., 2008).

Particle number concentrations exhibited the greatest temporal variability of all measured parameters (Fig. 1a). Mean nucleation- ($N_{10–30}$), Aitken- ($N_{30–100}$), and accumulation-mode ($N_{100–280}$) number concentrations were 3035 ± 3446, 3297 ± 2067, and 1500 ± 1208 cm^{-3}, respectively (Fig. S13). The nucleation mode exhibited the highest coefficient of variation (CV = 114 %), with daily $N_{10–30}$ maxima ranging from near-background concentrations to event peaks exceeding 15 000 cm^{-3}, characteristic of episodic NPF occurring against a low particle-number background (Kulmala et al., 2004). In contrast, the CS varied much less over the campaign averaging (8.96 ± 3.20) × 10^{-3} s^{-1}, with no significant difference between growth and non-growth days. This pronounced variability in $N_{10–30}$ despite relatively stable CS, motivates the detailed investigation of NPF processes discussed in Sect. 3.4.

Trace gases and VOCs reflected the mixed anthropogenic–biogenic character of the site (Fig. 1c, e, Fig. S11). NO_x (7.38 ± 4.69 ppb) exhibited the same dominant W/SW directional pattern as eBC, identifying vehicular traffic as the principal local source, whereas O_3 (23.9 ± 9.97 ppb) was enhanced in

https://doi.org/10.5194/egusphere-2026-4244
Preprint. Discussion started: 31 July 2026

photochemically aged sea-breeze air arriving from the S/SE (Fig. S7). NH_3 concentrations were relatively high (8.13 ± 3.27 ppb), consistent with its potential role in stabilizing H_2SO_4 clusters during ternary nucleation (Benson et al., 2011; Jung et al., 2008). In contrast, SO_2 exhibited the lowest mean concentration (0.30 ± 0.33 ppb) and frequently remained below the detection limit. Its pronounced temporal variability suggests that sulfuric acid formed via OH oxidation of SO_2 was influenced by intermittent transport from the industrial western sector rather than by a persistent regional source, implying that the contribution of H_2SO_4 to NPF may vary substantially over time and that condensable organic vapours could become increasingly important for sustaining particle growth (Donahue et al., 2013; Kupc et al., 2020). Oxygenated VOCs dominated the VOC burden (~60 %), with mean concentrations of acetone (2.93 ± 1.78 ppb), methanol (2.19 ± 1.02 ppb), and MVK + MACR (0.25 ± 0.18 ppb). Although biogenic VOC concentrations were lower (isoprene 0.77 ± 0.67 ppb; monoterpenes 0.053 ± 0.041 ppb), these compounds are potentially disproportionately important for NPF because of their high OH reactivity (Fig. S12) and efficient production of HOMs (Atkinson, 2003). Both isoprene and monoterpenes exhibited enhanced concentrations in air masses arriving from the W/NW sector, corresponding to the location of Guindy National Park and coincided with the dominant $N_{10–30}$ wind sector (Fig. S6). This spatial correspondence suggests that the park canopy is an important source of biogenic precursors contributing to particle formation and early particle growth.

https://doi.org/10.5194/egusphere-2026-4244
Preprint. Discussion started: 31 July 2026

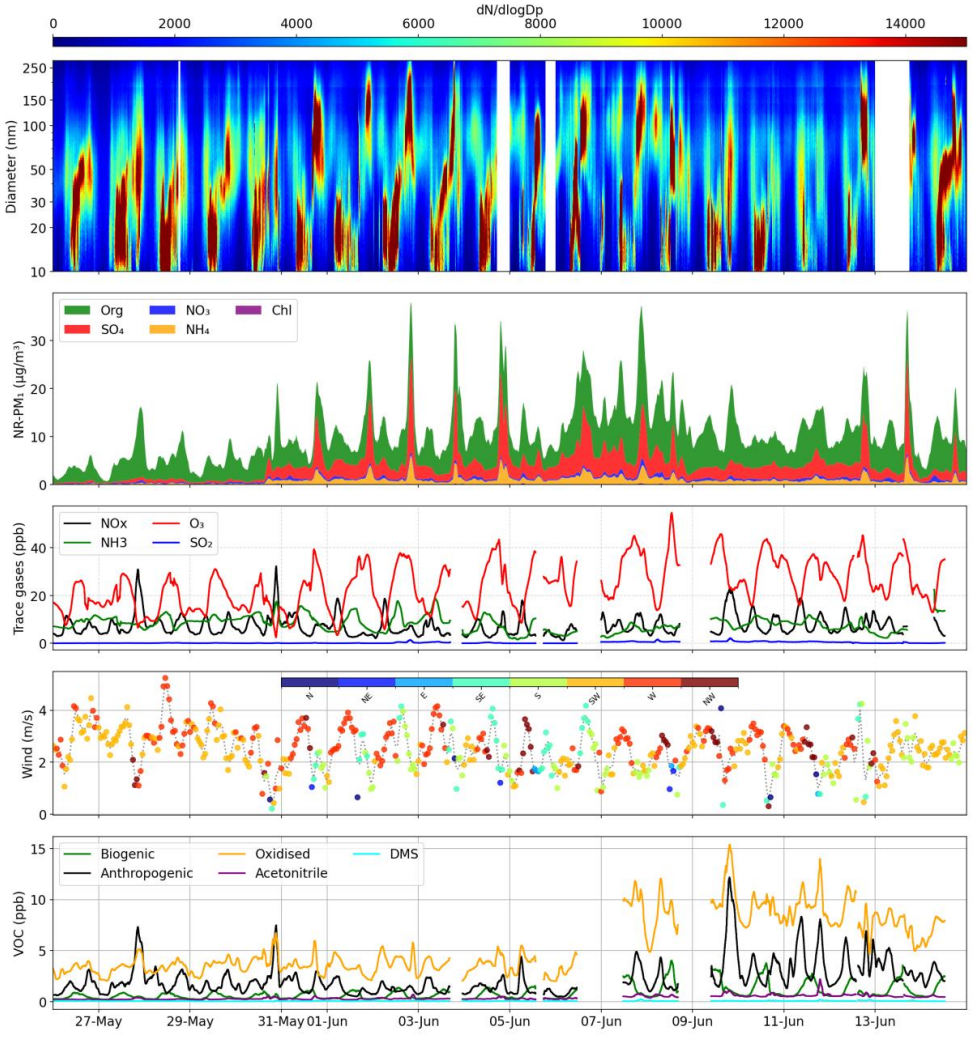

Figure 1. Time series of (a) particle number size distribution (dN/dlog D_p, cm^{-3}) measured by SMPS; (b) non-refractory PM_1 chemical composition (organics, sulfate, nitrate, ammonium, chloride; µg m^{-3}) measured by Q-ACSM; (c) trace gas concentrations (NO_x, O_3, NH_3, SO_2; ppb); (d) wind speed (m s^{-1}) and wind direction (colour axis) from the automated weather station; and (e) volatile organic compounds (VOCs) measured by PTR-TOF-MS, separated by source category: biogenic (green: isoprene + monoterpenes), oxygenated (yellow: methanol, acetone, MVK + MACR), and anthropogenic (black: benzene, toluene, xylenes). DMS (cyan) and acetonitrile (magenta) are shown separately. All data span 26 May–14 June 2025.

3.3 Diurnal Patterns and Atmospheric Processing

The mean diurnal cycles of particle number concentrations, gases, and aerosol chemical composition (Fig. 2) clearly distinguish photochemical processing from combustion-driven emissions at the site. The

https://doi.org/10.5194/egusphere-2026-4244
Preprint. Discussion started: 31 July 2026

nucleation mode ($N_{10–30}$) exhibited the most pronounced diurnal feature, increasing from near-background concentrations at approximately 06:00 IST to a sharp maximum between 10:00 and 11:00 IST before returning to background levels by approximately 14:00–15:00 IST (Fig. 2a). This recurring late-morning burst is the characteristic signature of photochemically driven NPF and indicates that conditions favourable for the production of freshly formed particles occur on a daily basis (Kulmala et al., 2004; Nieminen et al., 2018). The Aitken mode ($N_{30–100}$) displayed a broader maximum extending from midday into the evening (Fig. 2b) consistent with the condensational growth of newly formed particles at the growth rates reported in Sect. 3.4.4. In contrast, the accumulation mode ($N_{100–280}$) reached its maximum during the evening (Fig. 2c), reflecting the combined influences of traffic emissions, atmospheric aging, and coagulation rather than fresh particle formation (Kulmala et al., 2001). Organic aerosol, nitrate, chloride, and eBC exhibited bimodal diurnal cycles that closely tracked NO_x (Fig. 2m–r), confirming combustion as their dominant source, whereas sulfate showed only a weak diurnal cycle punctuated by occasional afternoon enhancements associated with airmasses arriving from the south and southeast.

Among trace gases, NO_x exhibited the classical urban bimodal rush-hour pattern, with a pronounced midday minimum resulting from boundary-layer development and photochemical loss (Fig. 2i). O_3 displayed the complementary photochemical diurnal cycle, increasing from morning NO titration to a midday-to-afternoon maximum of approximately 50 ppb (Fig. 2k; Monks et al., 2009), characteristic of the strongly oxidising tropical atmosphere. NH_3 remained elevated throughout the day, with a modest late-morning enhancement, whereas SO_2 exhibited no distinct diurnal cycle. Biogenic VOCs were strongly influenced by solar radiation: isoprene followed the canonical light- and temperature-dependent canopy emission pattern, increasing after approximately 08:00 IST and reaching a broad afternoon maximum (Fig. 2d; Fig. S9; Hu et al., 2015). This behaviour was mirrored by MVK + MACR and, at lower concentrations, by monoterpenes. In contrast, benzene, toluene and xylenes (BTX) aromatics exhibited a bimodal diurnal cycle closely aligned with traffic activity (Fig. 2e), confirming vehicular emissions as their dominant source (Tripathi et al., 2022; Wang et al., 2020). The temporal

https://doi.org/10.5194/egusphere-2026-4244
Preprint. Discussion started: 31 July 2026

353 offset between the late morning $N_{10–30}$ burst and the subsequent peak in biogenic precursor availability

354 and photochemical oxidation is examined mechanistically in Sect. 3.4.

355

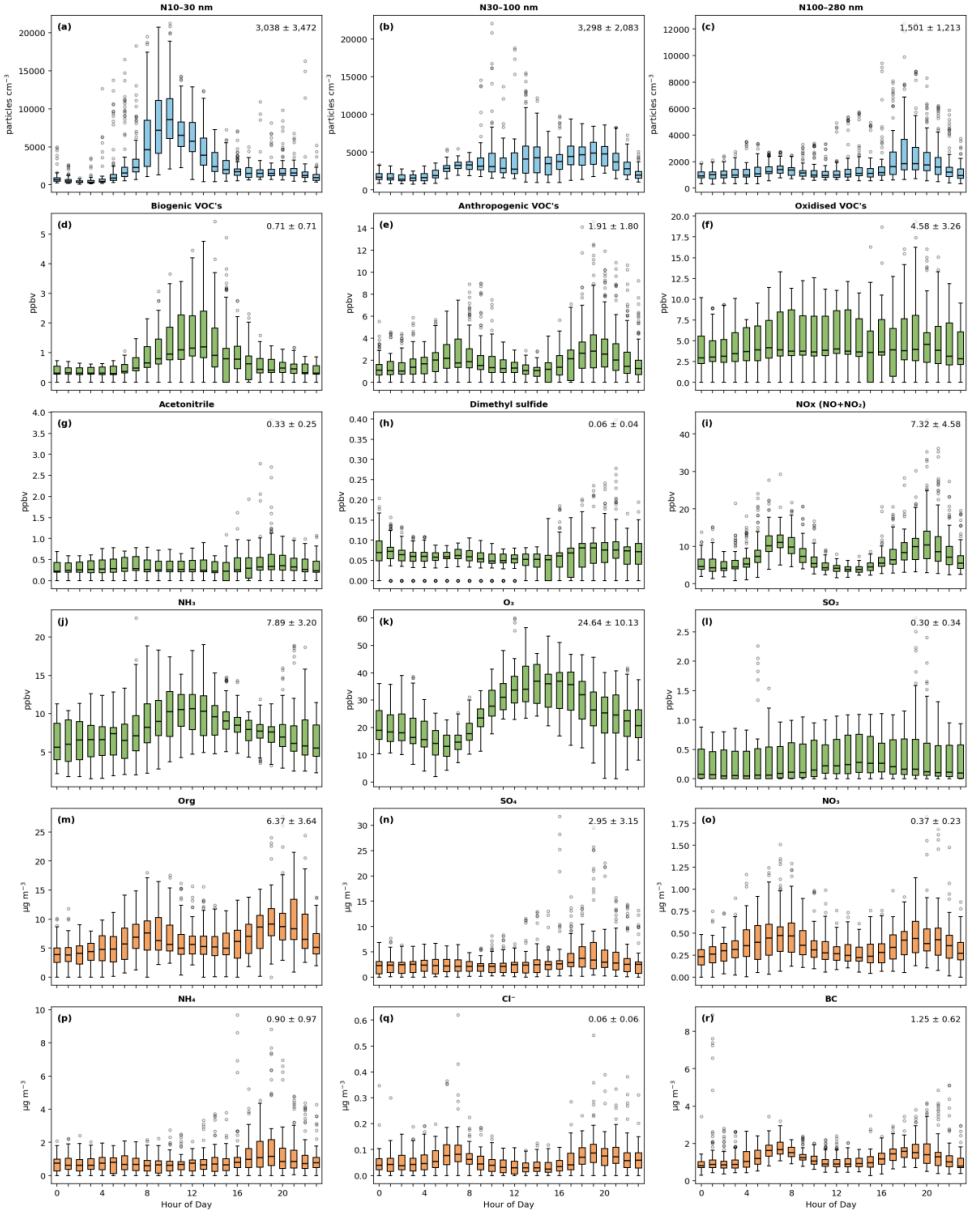

356

https://doi.org/10.5194/egusphere-2026-4244
Preprint. Discussion started: 31 July 2026

Figure 2. Hourly diurnal distributions of particle number concentrations, gaseous species, and aerosol chemical components. Box-and-whisker plots show the median (centre line), interquartile range (box), 5th–95th percentiles (whiskers), and outliers (circles). Panels (a–c): particle number concentrations in three SMPS size bins ($N_{10–30}$, $N_{30–100}$, $N_{100–280}$). Panels (d–f): VOC source classes (biogenic, anthropogenic, oxygenated). Panels (g–h): acetonitrile and DMS. Panels (i–l): trace gases (NO_x, NH_3, O_3, SO_2). Panels (m–q): non-refractory PM_1 components from Q-ACSM (organics, sulfate, nitrate, ammonium, chloride). Panel (r): equivalent black carbon at 880 nm. Box colours: blue – particle number; green – gas-phase species; orange – aerosol chemical components. The value shown in the upper-right corner of each panel represents the campaign-average concentration (mean ± 1 standard deviation)

3.4 Origin and Controls of NPF and growth events

3.4.1 Photochemical Secondary Origin of the Morning $N_{10–30}$ Enhancement

A pronounced $N_{10–30}$ enhancement was observed between approximately 07:00 and 11:00 IST on every day of the campaign (Fig. 2a, Fig. S13). To determine whether this increase originated from primary-emissions or secondary photochemical production, $N_{10–30}$ was normalised by two primary-emission tracers, eBC and NO_x, neither of which has a significant photochemical source. The $N_{10–30}$/eBC ratio increased from approximately 1000 during the pre-dawn baseline to approximately 8000 at 10:00 IST (an eightfold increase), while the $N_{10–30}/NO_x$ increased by approximately a factor of 25 over the same period (Fig. S18). Both ratios subsequently declined to near baseline values by 17:00–18:00 IST and remained low overnight. The eBC-normalized ratio provides the more robust diagnostic as eBC is essentially conserved on diurnal time scales whereas interpretation of the NO_x-normalized ratio is influenced both by particle production and by daytime photochemical removal of NO_x. Nevertheless, the $N_{10–30}/NO_x$ reached its maximum approximately 3 hours after the morning NO_x rush-hour peak (~07:00 IST, a delay consistent with the time scale required for OH-initiated oxidation of precursor vapours and subsequent particle formation, but inconsistent with direct co-emission from traffic sources. Together, these tracer-normalised diagnostics demonstrate that primary emissions cannot account for the observed morning enhancement in $N_{10–30}$ and indicate that it is dominated by secondary photochemical particle formation.

Two pre-dawn episodes on 1–2 June (Fig. S14) differed from the recurring daytime NPF. In both cases, $N_{10–30}$ peaks occurred before sunrise and coincided with elevated eBC, NO_x, and anthropogenic VOC concentrations, without the diurnal evolution characteristic of photochemically driven particle

https://doi.org/10.5194/egusphere-2026-4244
Preprint. Discussion started: 31 July 2026

formation. These episodes most likely reflect primary ultrafine particle emissions associated with early-morning heavy-duty vehicle activity and potentially other transient increases in traffic volume, although a secondary contribution cannot be completely excluded. While their origin cannot be unambiguously resolved with the available measurements, their occurrence before sunrise and their close association with combustion-tracers argue strongly against a photochemical NPF origin.

3.4.2 Event classification and growth

Following the classification scheme of Dal Maso et al. (2005), each campaign day was assigned to one of three categories based on the temporal evolution of the PNSD; full NPF with subsequent particle growth; partial events characterized by a nucleation-mode burst without sustained growth, and non-growth days. It is important to distinguish between two measures of the event occurrence. As established in Section 3.4.1, photochemically driven production of 10 to 30 nm particles occurred every day of the campaign. However, only 2 of the 20 days (10 %; 26 May and 14 June) satisfied the criteria for full NPF growth events, in which newly formed particles grew continuously from approximately 10 nm to 60–80 nm over several hours, producing the characteristic "banana-shaped" signature of regional NPF (Kulmala et al., 2004, 2012). On the remaining 18 days, although nucleation-mode particles formed, they failed to undergo sustained growth and the nucleation mode enhancement dissipated within 2–3 h.

3.4.3 Air-mass continuity, not scavenging, controls growth-event occurrence

The contrast between near-daily morning particle formation and the rarity of sustained particle growth narrows the controlling factor to one of three possibilities: the magnitude of morning particle formation, the strength of scavenging by pre-existing aerosols, or the sustained supply of condensable vapours required for growth beyond the nucleation mode. The magnitude of morning particle formation was indistinguishable between growth and non-growth days. Composite diurnal profiles of $N_{10–30}$/eBC and $N_{10–30}/NO_x$ for the two growth days and the eighteen non-growth days (Fig. S18) both reached their maxima at 10:00 IST and exhibited statistically indistinguishable peak values (Fig. S18). Likewise, the mean daily $N_{10–30}$ concentrations were nearly identical (3132 ± 3876 cm^{-3} on growth days vs. 3026 ±

https://doi.org/10.5194/egusphere-2026-4244
Preprint. Discussion started: 31 July 2026

3405 cm^{-3} on non-growth days). Although the non-growth composite exhibited a broader $N_{10–30}$ shoulder between 11:00 and 13:00 IST, the more rapid decline on growth days is consistent with particles growing out of the 10-30 nm size range rather than being removed predominantly by coagulation.

Pre-existing particle scavenging was likewise comparable between the two classes of days. The mean CS overlapped within one standard deviation for growth days (6.01×10^{-3} s^{-1} on 26 May and 9.24×10^{-3} s^{-1} on 14 June) and non-growth days ($(9.11 \pm 3.30) \times 10^{-3}$ s^{-1}). Similarly, the coagulation sink for a 10 nm particle was comparable between growth days (9.0×10^{-5} s^{-1} and 13.1×10^{-5} s^{-1}) and non-growth days ($(12.89 \pm 4.41) \times 10^{-5}$ s^{-1}; Fig. S13). The proxy-derived H_2SO_4 concentrations support the same conclusion. Sulfuric acid concentrations estimated using the parameterization of Mikkonen et al. (2011) (Fig. S19) were of the order of 10^6 molecules cm^{-3} for all day classes ($(0.99 \pm 2.18) \times 10^6$ on 26 May, $(2.32 \pm 3.64) \times 10^6$ on 14 June, and $(5.38 \pm 9.20) \times 10^6$ molecules cm^{-3} on non-growth days), well within the typical daytime boundary-layer range of 10^5–10^7 molecules cm^{-3} (Seinfeld, 2016). Notably, proxy H_2SO_4 concentrations were not elevated on growth days and, on average, were lower than on non-growth days, consistent with observations from subtropical sites in Taiwan where lower SO_2 concentrations were likewise reported during NPF growth days (Young et al., 2013). Taken together, the comparable condensation and coagulation sinks, together with the absence of enhanced H_2SO_4 during growth events, indicate that neither particle scavenging nor sulfuric acid availability distinguished growth from non-growth days. Instead, the suppression of particle growth despite comparable or higher proxy H_2SO_4 concentrations points to the availability of other low-volatility condensable vapours, most plausibly of organic origin, as the factor governing sustained particle growth.

The bulk aerosol chemical composition provides additional context for these findings. Accumulation-mode number concentrations ($N_{100–280}$) were lower on growth days (808 ± 343 cm^{-3}) than on non-growth days (1563 ± 1238 cm^{-3}), reflecting differences in air-mass origin discussed below rather than statistically distinguishable differences in bulk scavenging sinks. Likewise, sulfate concentrations were lower on growth days (0.62 ± 0.54 µg m^{-3}), than on non-growth days (3.14 ± 3.19 µg m^{-3}) consistent

https://doi.org/10.5194/egusphere-2026-4244
Preprint. Discussion started: 31 July 2026

with a stronger influence of the thermal power plant sector during non-growth periods and a greater accumulation of aged aerosol. Organic aerosol exhibited only a moderate difference (3.78 ± 2.82 vs. 6.60 ± 3.61 μg m^{-3}), while NO_x was slightly lower on growth days (6.12 ± 2.64 vs. 7.48 ± 4.80 ppb). Biogenic VOC concentrations were comparable between the two classes of days (isoprene: 0.66 ± 0.54 vs. 0.78 ± 0.68; monoterpenes: 0.052 ± 0.031 vs. 0.053 ± 0.042). Although, these differences are qualitatively consistent with somewhat more favorable conditions for particle growth on growth days, their magnitude is modest and does not explain the pronounced contrast in growth-event occurrence. Instead, they support the conclusion that the persistence of precursor supply, rather than differences in average aerosol composition or precursor abundance alone, governs whether newly formed particles undergo sustained growth.

The variable that clearly distinguished the two classes of days was air-mass continuity. On both growth days, surface winds remained within the W–NW continental sector from approximately 09:00 to 17:00 IST, sustaining an uninterrupted supply of biogenic precursor vapours from Guindy National Park and the upwind continental region. In contrast, in the eighteen non-growth days, surface winds shifted from the continental sector to the SE–E marine sector between 11:00 and 13:00 IST as the sea breeze developed (Fig. S3), interrupting the continental precursor supply at, or shortly after, the time of peak nucleation-mode formation. Taken together, these observations indicate that the canonical CS limitation framework alone is insufficient to explain the growth event at this site. During the pre-monsoon to monsoon-onset transition at the Chennai urban-forest interface, sustained particle growth is more strongly associated with the continuity of precursor supply than with differences in particle formation intensity or scavenging by pre-existing aerosols. These findings suggest that strategies aimed solely at reducing primary aerosol loading, and hence CS, may have only a limited influence on the frequency of successful particle-growth events unless accompanied by changes in the availability and continuity of gas-phase precursor vapours.

3.4.4 Particle Growth Rates on complete NPF days

The two full NPF growth events exhibited sustained particle growth from the nucleation mode into the Aitken mode over several hours. On 26 May 2025, NPF commenced at ~11:00 IST, later than the typical

https://doi.org/10.5194/egusphere-2026-4244
Preprint. Discussion started: 31 July 2026

onset time of around ~09:00 IST because morning cloud cover reduced incoming solar radiation (Fig. S4); precipitation recorded at nearby stations is consistent with these cloudy conditions. In contrast, the 14 June 2025 event began at ~09:00 IST under clear-sky conditions with strong solar insolation. On both days, particle growth continued until ~17:00 IST, after which changes in wind-direction and increasing traffic emissions disrupted the continuity of the particle number size distributions. To avoid these influences, growth rates were calculated only up to 16:00 IST.

The derived growth rates were 4.53 nm h^{-1} on 26 May and 3.43 nm h^{-1} on 14 June (Fig. S10), well within the typical range of 2–10 nm h^{-1} reported for continental boundary-layer environments (Kanawade et al., 2022; Kerminen et al., 2018). A comparison of the growth rate, J, and CS with values reported for urban, coastal, forest, mountain, rural, and polluted environments worldwide is presented in Table 1. Such comparisons should be interpreted cautiously because of differences among studies in particle-size ranges, instrumentation, and event-selection criteria. Although the 26 May event began later, with a geometric mean diameter (GMD) of 25 nm at 11:09 IST, particle population grew to 45.7 nm by 15:58 IST. On 14 June, the GMD increased from 25.5 nm at 08:58 IST to 50.2 nm at 15:58 IST (Fig. 3). The larger final particle size on 14 June is consistent with the longer uninterrupted growth period associated with sustained continental airflow.

https://doi.org/10.5194/egusphere-2026-4244
Preprint. Discussion started: 31 July 2026

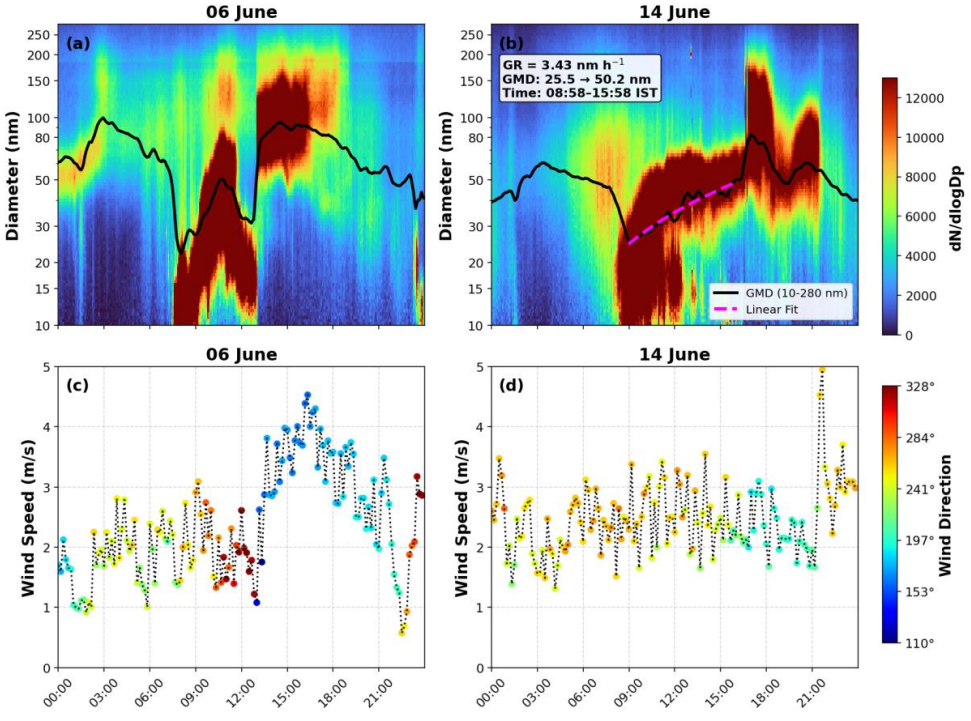

Figure 3. Time evolution of the particle number size distribution and meteorological conditions on a non-event day (6 June 2025) and a complete NPF event day (14 June 2025). Panels (a, b): contour plots of dN/dlog D_p as a function of time and particle diameter, with geometric mean diameter (GMD) overlaid (black line). On 14 June, the linear growth phase used to derive the growth rate (GR = 3.43 nm h^{-1} between 08:58 and 15:58 IST) is indicated by the pink dashed line. Panels (c, d): corresponding wind speed (m s^{-1}) and wind direction (colour-coded) for the same periods.

3.5 Source Apportionment and Chemical Drivers of NPF

PMF was applied to the combined dataset comprising particle number size distributions, aerosol chemical composition, trace gases, and VOCs to identify the principal source factors associated with NPF. A six-factor solution was selected based on statistical robustness and physical interpretability. The resolved factor profiles are shown in Fig. 4a–f, and their normalized diurnal variations are presented in Fig. 4g–l.

3.5.1 Factor Profiles and Source Identification

Factor 1 – NPF / nucleation burst. Factor 1 (F1) is overwhelmingly dominated by $N_{10–30}$ which accounts for 73.8 % of its contribution, with secondary contributions from isoprene (20.9 %), $N_{30–100}$

https://doi.org/10.5194/egusphere-2026-4244
Preprint. Discussion started: 31 July 2026

(13.0 %), monoterpenes (13.0 %), and MVK + MACR (13.0 %) (Fig. 4a). Contributions from combustion tracers (eBC: 1.8 %; NO_x: 0.8 %) and inorganic aerosol species (SO_4^{2-}: 5.5 %; NH_4^+: 6.2 %) are minimal. F1 uniquely explains the majority of the nucleation-mode particle number, $N_{10–30}$ with the next largest factor contributing only 21.1 %, identifying it as the factor most strongly associated with photochemically produced nucleation-mode particles. The co-loading of biogenic VOCs is consistent with an important contribution from oxidation products of biogenic VOCs to particle formation and early condensational growth (Riccobono et al., 2014; Tröstl et al., 2016). The diurnal profile of F1 (Fig. 4g) is the most distinct of the six factors, increasing rapidly from background concentrations at ~06:00 IST, peaking near ~10:00 IST, and returning to baseline by ~14:00 IST. The weekday and weekend profiles are essentially identical (Fig. S15), providing independent evidence that NPF at this site is primarily governed by photochemical processing and biogenic precursor availability rather than by variations in anthropogenic emission activity, consistent with the photochemically controlled urban regime proposed by Kulmala et al. (2017) for environments influenced by nearby natural vegetation.

Factor 2 – Vehicular traffic / primary urban combustion. Factor 2 (F2) is characterized by high contributions from NO_x (48.8 %), $N_{30–100}$ (44.0 %), benzene (43.4 %), eBC (40.9 %), NH_3 (37.2 %), xylenes (35.7 %), $N_{100–280}$ (27.5 %), DMS (23.8 %), and toluene (23.4 %) (Fig. 4b), and uniquely explains the largest fractions of $N_{30–100}$, eBC, and NO_x. The co-occurrence of BTX aromatics, eBC, and –NO_x is the characteristic fingerprint of gasoline and diesel vehicular emissions in Indian urban environments (Dumka et al., 2018; Sahu et al., 2016), consistent with the dominant W/SW directional pattern shown by the pollution wind roses (Fig. S16). The NH_3 and DMS co-loadings likely reflect nearby anthropogenic sources. The 21% contribution of F2 to $N_{10–30}$ is less straightforward to interpret and may include both primary ultrafine particle emissions and secondary particles formed contemporaneously with traffic emissions. The bimodal diurnal profile (Fig. 4h), with peaks at ~07:00 and ~19:00 IST, and a weaker weekday morning peak on weekends (Fig. S15) is characteristic of commuter traffic. From the perspective of NPF, F2 represents a transient morning combustion influence that precedes the photochemical nucleation burst. Morning rush-hour eBC and primary-particle loading

https://doi.org/10.5194/egusphere-2026-4244
Preprint. Discussion started: 31 July 2026

elevate the CS and scavenge condensable vapours before they can participate in nucleation (Sipilä et al., 2010), but the post-08:00 IST decline of F2 with boundary-layer development reduces both the coagulation sink for freshly forming clusters and the scavenging of condensable precursors before the NPF burst onset.

Factor 3 – Biogenic / photochemical precursor reservoir. Factor 3 (F3) simultaneously dominates ten species: O_3 (74.1 %), MVK + MACR (62.0 %), monoterpenes (59.8 %), SO_2 (58.4 %), isoprene (56.2 %), NH_3 (50.2 %), methanol (47.7 %), acetone (45.2 %), acetonitrile (41.0 %), and DMS (26.8 %; Fig. 4c). This breadth indicates not a single point source but a photochemically active air-mass state in which biogenic canopy emissions, their gas-phase oxidation products, and inorganic precursors are co-processed under high solar radiation. The W/NW continental origin (Fig. S16) is consistent with photo-oxidation of emissions from the nearby Guindy National Park within the urban airshed. F3 constitutes the essential precursor reservoir for NPF, supplying SO_2 for H_2SO_4 production (OH + SO_2), NH_3 for ternary cluster stabilization, and the biogenic organic vapour pool (isoprene, monoterpenes, MVK + MACR) from which HOMs are produced through OH- and O_3-initiated oxidation (Bianchi et al., 2019; Tröstl et al., 2016). The F3 diurnal profile (Fig. 4i) shows a broad midday maximum from ~11:00 to 15:00 IST, ~3 h after the F1 burst at ~10:00 IST. This lag reflects both the photochemical buildup of oxidants and low-volatility products and the condensational growth timescale required for freshly nucleated particles to reach the $N_{10–30}$ detection window at the observed growth rate.

Factor 4 – Aged urban aromatic VOC plume. Factor 4 (F4) uniquely dominates the three BTX species (xylenes: 57.1 %; toluene: 56.0 %; benzene: 49.9 %) alongside oxygenated VOCs (acetone: 39.5 %; MVK + MACR: 23.4 %), with near-absent eBC (Fig. 4d). The elevated BTX-to-NO_x ratio and the absence of eBC distinguish F4 from F2 (fresh vehicular exhaust) and identify it as an aged aromatic plume. The SO_2 co-loading (26.6 %) is consistent with a mixed industrial–petrochemical fingerprint. BTX photo-oxidation generates HOMs and highly oxygenated aromatic products capable of contributing to nucleation and SOA growth (Molteni et al., 2018; Ng et al., 2007). The F4 diurnal pattern (Fig. 4j) is dominant in the evening ~19:00 IST, consistent with nocturnal boundary-layer accumulation

https://doi.org/10.5194/egusphere-2026-4244
Preprint. Discussion started: 31 July 2026

of industrial aromatic emissions, with a weekend enhancement suggesting additional residential and recreational contributions (Warneke et al., 2013).

Factor 5 – Aged secondary aerosol associated with combustion plumes. Factor 5 (F5) uniquely dominates chloride (76.0 %), NO_3^- (67.1 %), and organics (66.3 %), with co-loadings of eBC (38.3 %) and $N_{100–280}$ (26.7 %; Fig. 4e). The chloride–acetonitrile signature points to a biomass- or plastic-combustion origin (Gunthe et al., 2021), while the high NH_4NO_3 contribution (which requires atmospheric aging to form) and the accumulation-mode dominance identify F5 as processed, internally mixed secondary aerosol rather than fresh smoke. F5 acts as a modulating rather than a dominant control on NPF, contributing to elevated-CS episodes but consistent with the broader observation that CS is not the discriminating variable between growth and non-growth days at this site.

Factor 6 – Regional secondary sulfate. Factor 6 (F6) is dominated by SO_4^{2-} (74.3 %) and NH_4^+ (70.9 %) in a near-equimolar ratio consistent with $(NH_4)_2SO_4$, with co-loadings of DMS (19.1 %) and O_3 (18.2 %) (Fig. 4f). The DMS pollution wind rose (Fig. S7) shows a smaller component from the SE sector, providing observational evidence of a marine biogenic component. F6 acts as a secondary NPF inhibitor through its accumulation-mode CS (correlation with F1: $r = -0.23$, $p < 0.001$) and peaks between ~18:00 and 20:00 IST, the time at which marine-sector winds typically reach the receptor site.

3.5.2 Mechanistic Framework: Inter-Factor Couplings

Beyond the diurnal behaviour of individual factors, the PMF analysis reveals three relationships between source factors that are not evident from species-level observations alone and that directly support the formation–survival interpretation developed in Sect. 3.4. First, the NPF factor (F1) is weekday–weekend invariant (Fig. S15), confirming that nucleation-mode production is decoupled from the diurnal cycle of anthropogenic activity. Second, F1 and the traffic factor (F2) are negatively correlated ($r = -0.41$; Fig. S17), consistent with morning boundary-layer development diluting the CS as a necessary precondition for the NPF burst, rather than CS reduction being the discriminating variable for growth. Third, F5 and F6 are positively correlated ($r = +0.41$) and both peak during sea-breeze and monsoon-onset episodes, reinforcing the air-mass-origin control identified in Sect. 3.4.

https://doi.org/10.5194/egusphere-2026-4244
Preprint. Discussion started: 31 July 2026

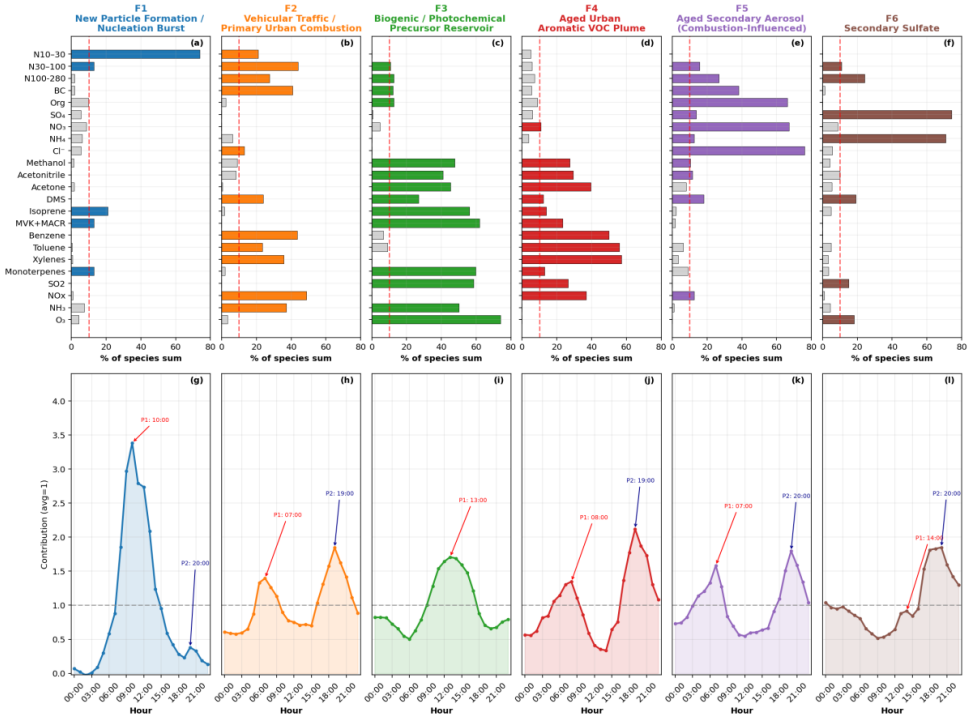

Figure 4. Six-factor PMF solution. Panels (a–f) show the percentage contribution of each input species to Factors 1–6, respectively; the dashed vertical line at 10 % marks the threshold used to identify dominant species. Panels (g–l) show the corresponding diurnal profiles of each factor, normalised to unit area to allow comparison across factors with different absolute magnitudes. P1 and P2 denote the primary and secondary diurnal peaks, respectively, with the annotated times indicating the occurrence of each peak. Annotated peak times indicate the dominant period of influence for each factor. Factor identifications: Factor 1 — NPF / nucleation burst; Factor 2 — vehicular traffic / primary urban combustion; Factor 3 — biogenic / photochemical precursor reservoir; Factor 4 — aged urban aromatic VOC plume; Factor 5 — aged secondary aerosol associated with combustion plumes; Factor 6 — regional secondary sulfate.

3.6 Synthesis and atmospheric implications

The evidence assembled here defines a regime in which the canonical CS-limitation framework for NPF in polluted environments (Kulmala et al., 2017) does not capture growth-event occurrence at this site. Photochemical secondary particle formation in the 10–30 nm range was a daily feature of the campaign, with morning peaks of comparable magnitude on growth and non-growth days. CS, CoagS, and $J_{10\text{-}30}$ were statistically indistinguishable between these days. The contrast in growth-event occurrence (2 of 20 days) is therefore not explained by formation rate or by aerosol scavenging. The discriminating

https://doi.org/10.5194/egusphere-2026-4244
Preprint. Discussion started: 31 July 2026

variable is air-mass continuity. Complete growth events occurred on days when continental biogenic precursor supply persisted through the 10:00–17:00 IST window, and failed when the developing sea-breeze redirected the receptor air mass to the marine and anthropogenic aerosols from the thermal power plant sector before growth could complete.

Mechanistic interpretation must be drawn cautiously in the absence of direct H_2SO_4 or HOM measurements. Three observational constraints nonetheless point to biogenic-organic vapours as the operative growth pathway. The W/NW enhancement of monoterpenes and isoprene co-located with Guindy National Park, placing a localised biogenic source upwind of the receptor; the dominance of monoterpene oxidation in the daytime OH-reactivity budget despite lower mixing ratios than isoprene; and the lower SO_2 and NO_x concentrations on growth days, consistent with reduced NO_x-mediated suppression of HOM formation (Lehtipalo et al., 2018; Ng et al., 2007). These are associations between precursor environment and event outcome rather than direct mechanistic proofs.

Two broader implications follow. First, in tropical coastal megacities with adjacent biogenic sources, a configuration shared by many South and Southeast Asian urban centres, NPF event frequency may be governed by precursor-supply continuity rather than CS, displacing the conventional paradigm for this class of environment. Second, regional climate and air-quality models that parameterise NPF suppression through CS alone will under-represent NPF variability over coastal South Asia unless sea-breeze and monsoon-transition dynamics are explicitly resolved. Future deployment of advanced aerosol instruments to chemically resolve sub 10 nm sized aerosols, combined with multi-seasonal monitoring, will be needed to constrain the molecular-level mechanism and test the air-mass-continuity hypothesis across a larger event population.

https://doi.org/10.5194/egusphere-2026-4244
Preprint. Discussion started: 31 July 2026

623
624
625

Table 1: Comparison of key NPF characteristics reported in the present study and previous studies conducted across diverse environments worldwide, including urban, coastal, forest, mountain, rural, and highly polluted regions. Reported parameters include particle growth rate, particle number size distribution (PNSD) range used for growth-rate determination, particle formation rate (J) and the corresponding particle size at which it was calculated, and CS. Differences among studies should be interpreted with caution because the particle-size ranges used for calculating growth and formation rates, instrumental configurations, event-selection criteria, and analysis methodologies vary between studies.

Study	Location	Site type	Growth rate ($nm\ h^{-1}$)	PNSD used (nm)	Formation rate ($cm^{-3}\ s^{-1}$)	Size for formation rate	Condensation sink (s^{-1})
Present study	Chennai, India	Urban tropical forest / coastal	4.53 and 3.43	10–280	0.52 and 0.96	10-30	6.01×10^{-3} and 9.24×10^{-3}
Sebastian et al. (2021)	Ranichauri, India	Mountain background	8.51 ± 4.46, 4.86 ± 3.13	10–25	0.09 ± 0.08, 0.26 ± 0.27	10	-
Yu et al. (2014)	Ozark Forest, USA	Forest	4.7 ± 2.6	5–25	11.0 ± 10.6, 1.0 ± 1.1	1nm, 5nm	~4 to 12×10^{-3}
Varghese et al. (2020)	Solapur, India	Rural rain shadow	1.2 to 13.8	15–30	0.2 to 10.0	15nm	6.47 to 30.38×10^{-3}
Kanawade et al. (2014b)	Pune & Kanpur, India	Urban	6.5 ± 1.2, 8.7 ± 3.2	5–25	1.5 ± 1.0, 7.2 ± 3.3	J_5	$16.2 \pm 7.1 \times 10^{-3}$, $33.3 \pm 8.7 \times 10^{-3}$
Young et al. (2013)	Central Taiwan	Urban, coastal, mountain, downwind	7.4 to 24	10–25	4.4 to 30	10nm	1.6 to 3.9×10^{-2}
Bousiotis et al. (2021a)	13 sites across Europe	Rural background, urban background, roadside	2.87 to 5.17	Up to 30 or 50	4.90×10^{-3} to 1.38×10^{-1}	J_{10}, J_{16}	Variable
Bousiotis et al. (2021b)	16 sites across Europe	Rural background, urban background, roadside	2.87 to 5.5	Up to 30 or 50	8.69×10^{-3} to 1.02×10^{-1}	10nm, 16nm	2.32×10^{-3} to 3.10×10^{-2}
Baalbaki et al. (2021)	Agia Marina Xyliatos, Cyprus	Rural background	3.7 to 11.7	1.5–20	6.42 ± 8.47	$J_{1.5}$, J_3, J_7	~10^{-3} to 10^{-2}
Sebastian et al. (2022)	6 sites in India	Mountain, urban, coastal	0.2 to 17.2	5–15 to 25	Variable	J 5 to J15	7.9 to 16.1×10^{-3}
Dal Maso et al. (2005)	Hyytiälä, Finland	Boreal forest	3	3–25	0.8	J 3	2.4×10^{-3} (events), 7.0×10^{-3} (non-events)
Ali et al. (2025)	Delhi, India	Urban	3.2 to 10.0	10–25	2.19, 136	J_{10}, $J_{1.5}$	0.02 to 0.06
Yu et al. (2017)	Highly polluted environments	Highly polluted urban	0.1 to 38.3	>3	0.24 to 5000	Variable	0.006 to 0.34
Singh et al. (2025b)	Tehri Garhwal, Uttarakhand, India	Mountain, Rural background	1.29 ± 0.20	10-25	0.04 ± 0.03	11.5 nm	(11.91 ± 3.13) × 10^{-3}

https://doi.org/10.5194/egusphere-2026-4244
Preprint. Discussion started: 31 July 2026

4 Conclusion

We characterised NPF and subsequent particle growth over 20 days at an urban forest–coastal interface in Chennai, combining PNSD, NR-PM_1 composition, VOCs, trace gases, and PMF source apportionment. Photochemically driven formation of 10–30 nm particles occurred on every day of the campaign and was clearly decoupled from primary emissions, as evidenced by pronounced morning increases in $N_{10–30}$/eBC and $N_{10–30}/NO_x$. Sustained growth into the accumulation mode, however, occurred on only 2 of 20 days with growth rates of 4.53 and 3.43 nm h^{-1}. The particle formation rate, CS, and CoagS were statistically indistinguishable between growth and non-growth days, while proxy H_2SO_4 concentrations were, on average, higher on non-growth days. Instead, successful growth coincided with uninterrupted W/NW continental flow from the adjacent forest sector and terminated when the sea breeze redirected transport to marine air. PMF attributed 73.8 % of the variance in $N_{10–30}$ to a factor co-loaded with isoprene, monoterpenes, and MVK + MACR that showed no weekday–weekend dependence and was negatively correlated with the vehicular traffic factor ($r = -0.41$). Collectively, these observations indicate that the nucleation-mode particle population at this site is most consistently associated with the photo-oxidation of biogenic precursors, while successful growth appears to depend primarily on the temporal continuity of precursor supply rather than on sulfuric acid availability or aerosol scavenging.

Biogenic organic vapours are an established driver of NPF in vegetated and remote environments, including boreal forests (Dal Maso et al., 2005), isoprene-dominated temperate forests (Yu et al., 2014), and chamber experiments demonstrating nucleation and early growth from oxidised terpene vapours (Riccobono et al., 2014). In contrast, urban NPF has been attributed predominantly to anthropogenic precursors, including H_2SO_4 stabilised by ammonia and amines in Chinese megacities (Tang et al., 2025; Yang et al., 2026), sulfuric acid together with anthropogenic low-volatility organics in Houston (Tiszenkel et al., 2025), and nocturnal biomass-burning emissions in Delhi (Mishra et al., 2023). Likewise, coastal NPF has more commonly been linked to marine and tidal sources (O'Dowd et al., 2002), whereas marine-sector air at our site suppressed rather than promoted particle growth. Previous

https://doi.org/10.5194/egusphere-2026-4244
Preprint. Discussion started: 31 July 2026

observations at this location similarly attributed a rapid growth event to sulfate associated with nearby power plant emissions (Singh et al., 2023). By combining chemically resolved gas- and particle-phase measurements with PMF source apportionment under representative atmospheric conditions, our results instead demonstrate a strong association between the nucleation-mode particle population and biogenic VOCs originating from the protected forest. Although this association does not by itself establish causality, it is supported independently by the air-mass analysis, the absence of a weekday-weekend effect, and the negative relationship with the vehicular traffic factor. Collectively, these findings suggest that Chennai represents an uncommon example of a densely populated coastal mega city in which NPF is associated with biogenic rather than an anthropogenic or marine, precursor pool, sustained by vegetation.

These conclusions should be interpreted in the context of several limitations. The study spans only 20 days and includes two complete growth events, limiting the statistical robustness of comparisons between growth and non-growth regimes. The 10 nm lower detection limit of the SMPS precludes direct observation of the initial nucleation process, while the absence of direct measurements of sulfuric acid (H_2SO_4) and highly oxygenated organic molecules (HOMs) prevents definitive identification of the nucleating vapours. In addition, PMF apportions statistical covariance among measured species rather than uniquely identifying physical particle sources; consequently, the resolved factors are more appropriately interpreted as characteristic atmospheric process states than as discrete emission sources.

Despite these limitations, the consistency between the PMF analysis, air-mass trajectories, and meteorological evolution suggests that successful particle growth at this urban forest–coastal interface depends more strongly on the continuity of precursor supply than on the magnitude of the condensation sink alone. If this mechanism proves to be representative of tropical coastal megacities, NPF variability will depend not only on aerosol loading but also on mesoscale meteorology controlling precursor transport, particularly sea-breeze circulation and monsoon-

https://doi.org/10.5194/egusphere-2026-4244
Preprint. Discussion started: 31 July 2026

transition dynamics. Models that parameterise NPF suppression solely through the condensation sink may therefore underestimate this variability, and reductions in aerosol loading may not necessarily increase the frequency of successful growth events if precursor continuity remains the limiting factor. Multi-season, chemically resolved measurements extending below 10 nm, together with direct observations of sulfuric acid and HOMs, are now needed to determine the prevalence of this mechanism across tropical coastal environments.

Acknowledgements

The authors acknowledge the help of Mathew Sebastian in calculating different parameters from the SMPS data. We also acknowledge Shakeel Ahmed Lone for his assistance with ACSM data analysis. The authors further acknowledge the use of OpenAI's ChatGPT and Anthropic's Claude AI assistants for improving the language, clarity, and readability of the manuscript.

Data availability

The datasets generated and analysed during this study are publicly available from Zenodo at https://doi.org/10.5281/ZENODO.21355747 (Devaprasad et al., 2026a).

Competing interests

The authors declare that they have no conflict of interest.

Author Contribution

SSG conceived the study, planned the field campaign, and arranged funding. AMS, RS, and SD conducted the field campaign with assistance from MD, YS, GRM, TKJ, SS, and IA. MD analyzed the data and wrote the manuscript with input from PL, GP, RR, and SSG. GP, AMS, SD and GRM reviewed and edited the manuscript. GRM and TKJ performed the literature survey and compiled the data.

https://doi.org/10.5194/egusphere-2026-4244
Preprint. Discussion started: 31 July 2026

Financial support

This research received no specific grant from any funding agency in the public, commercial, or not-for-profit sectors.

https://doi.org/10.5194/egusphere-2026-4244
Preprint. Discussion started: 31 July 2026

References

Ali, U., Singh, V., Faisal, M., Kumar, M., and Gani, S.: Exploring the influence of physical and chemical factors on new particle formation in a polluted megacity, Environ. Sci. Atmos., 5, 25–47, https://doi.org/10.1039/D4EA00114A, 2025.

Atkinson, R.: Kinetics of the gas-phase reactions of OH radicals with alkanes and cycloalkanes, Atmos. Chem. Phys., 3, 2233–2307, https://doi.org/10.5194/acp-3-2233-2003, 2003.

Backman, J., Rizzo, L. V., Hakala, J., Nieminen, T., Manninen, H. E., Morais, F., Aalto, P. P., Siivola, E., Carbone, S., Hillamo, R., Artaxo, P., Virkkula, A., Petäjä, T., and Kulmala, M.: On the diurnal cycle of urban aerosols, black carbon and the occurrence of new particle formation events in springtime São Paulo, Brazil, Atmos. Chem. Phys., 12, 11733–11751, https://doi.org/10.5194/acp-12-11733-2012, 2012.

Benson, D. R., Yu, J. H., Markovich, A., and Lee, S.-H.: Ternary homogeneous nucleation of H_2SO_4, NH_3, and H_2O under conditions relevant to the lower troposphere, Atmos. Chem. Phys., 11, 4755–4766, https://doi.org/10.5194/acp-11-4755-2011, 2011.

Bianchi, F., Kurtén, T., Riva, M., Mohr, C., Rissanen, M. P., Roldin, P., Berndt, T., Crounse, J. D., Wennberg, P. O., Mentel, T. F., Wildt, J., Junninen, H., Jokinen, T., Kulmala, M., Worsnop, D. R., Thornton, J. A., Donahue, N., Kjaergaard, H. G., and Ehn, M.: Highly Oxygenated Organic Molecules (HOM) from Gas-Phase Autoxidation Involving Peroxy Radicals: A Key Contributor to Atmospheric Aerosol, Chem. Rev., 119, 3472–3509, https://doi.org/10.1021/acs.chemrev.8b00395, 2019.

Cappellin, L., Karl, T., Probst, M., Ismailova, O., Winkler, P. M., Soukoulis, C., Aprea, E., Märk, T. D., Gasperi, F., and Biasioli, F.: On Quantitative Determination of Volatile Organic Compound Concentrations Using Proton Transfer Reaction Time-of-Flight Mass Spectrometry, Environ. Sci. Technol., 46, 2283–2290, https://doi.org/10.1021/es203985t, 2012.

Chu, B., Kerminen, V.-M., Bianchi, F., Yan, C., Petäjä, T., and Kulmala, M.: Atmospheric new particle formation in China, Atmos. Chem. Phys., 19, 115–138, https://doi.org/10.5194/acp-19-115-2019, 2019.

Dal Maso, M., Kulmala, M., Lehtinen, K. E. J., Mäkelä, J. M., Aalto, P., and O'Dowd, C. D.: Condensation and coagulation sinks and formation of nucleation mode particles in coastal and boreal forest boundary layers, J. Geophys. Res. Atmos., 107, https://doi.org/10.1029/2001JD001053, 2002.

Dal Maso, M., Kulmala, M., Riipinen, I., Wagner, R., Hussein, T., Aalto, P. P., and Lehtinen, K. E. J.: Formation and growth of fresh atmospheric aerosols: eight years of aerosol size distribution data from SMEAR II, Hyytiälä, Finland, Boreal Environ. Res., 10, 323–336, 2005.

Devaprasad, M., Amrutha, M. S., Joshi, T. K., Dey, S., Malavika, G. R., Sapkota, Y., Salim, R., Srivastava, S., Amin, I., Pandithurai, G., Raghunathan, R., Liu, P., and Gunthe, S. S.: Dataset for atmospheric new particle formation measurements over the IIT Madras campus during May–June 2025, https://doi.org/10.5281/ZENODO.21355747, 2026a.

Devaprasad, M., Rastogi, N., Sharma, K., Attri, P., Mohanty, R. K., Harithasree, S., Singh, A., Yadav, S., Tiwari, D. M., Laskar, A. H., Dabhi, A., Bhushan, R., Das, S. K., and Sudheer, A. K.: Spatiotemporal Variations in Fossil vs Non-Fossil Source Contributions to Carbonaceous Aerosols across Diverse Indian Environments: An Assessment via Radiocarbon, ACS Earth Space Chem., 10, 1439–1452, https://doi.org/10.1021/acsearthspacechem.6c00055, 2026b.

Donahue, N. M., Ortega, I. K., Chuang, W., Riipinen, I., Riccobono, F., Schobesberger, S., Dommen, J., Baltensperger, U., Kulmala, M., Worsnop, D. R., and Vehkamaki, H.: How do organic vapors

https://doi.org/10.5194/egusphere-2026-4244
Preprint. Discussion started: 31 July 2026

contribute to new-particle formation?, Faraday Discuss., 165, 91, https://doi.org/10.1039/c3fd00046j, 2013.

Drinovec, L., Močnik, G., Zotter, P., Prévôt, A. S. H., Ruckstuhl, C., Coz, E., Rupakheti, M., Sciare, J., Müller, T., Wiedensohler, A., and Hansen, A. D. A.: The "dual-spot" Aethalometer: an improved measurement of aerosol black carbon with real-time loading compensation, Atmos. Meas. Tech., 8, 1965–1979, https://doi.org/10.5194/amt-8-1965-2015, 2015.

Du, W., Cai, J., Zheng, F., Yan, C., Zhou, Y., Guo, Y., Chu, B., Yao, L., Heikkinen, L. M., Fan, X., Wang, Y., Cai, R., Hakala, S., Chan, T., Kontkanen, J., Tuovinen, S., Petäjä, T., Kangasluoma, J., Bianchi, F., Paasonen, P., Sun, Y., Kerminen, V.-M., Liu, Y., Daellenbach, K. R., Dada, L., and Kulmala, M.: Influence of Aerosol Chemical Composition on Condensation Sink Efficiency and New Particle Formation in Beijing, Environ. Sci. Technol. Lett., 9, 375–382, https://doi.org/10.1021/acs.estlett.2c00159, 2022.

Dumka, U. C., Kaskaoutis, D. G., Tiwari, S., Safai, P. D., Attri, S. D., Soni, V. K., Singh, N., and Mihalopoulos, N.: Assessment of biomass burning and fossil fuel contribution to black carbon concentrations in Delhi during winter, Atmos. Environ., 194, 93–109, https://doi.org/10.1016/j.atmosenv.2018.09.033, 2018.

Gordon, H., Kirkby, J., Baltensperger, U., Bianchi, F., Breitenlechner, M., Curtius, J., Dias, A., Dommen, J., Donahue, N. M., Dunne, E. M., Duplissy, J., Ehrhart, S., Flagan, R. C., Frege, C., Fuchs, C., Hansel, A., Hoyle, C. R., Kulmala, M., Kürten, A., Lehtipalo, K., Makhmutov, V., Molteni, U., Rissanen, M. P., Stozkhov, Y., Tröstl, J., Tsagkogeorgas, G., Wagner, R., Williamson, C., Wimmer, D., Winkler, P. M., Yan, C., and Carslaw, K. S.: Causes and importance of new particle formation in the present-day and preindustrial atmospheres, J. Geophys. Res. Atmos., 122, 8739–8760, https://doi.org/10.1002/2017JD026844, 2017.

Gunthe, S. S., Liu, P., Panda, U., Raj, S. S., Sharma, A., Darbyshire, E., Reyes-Villegas, E., Allan, J., Chen, Y., Wang, X., Song, S., Pöhlker, M. L., Shi, L., Wang, Y., Kommula, S. M., Liu, T., Ravikrishna, R., McFiggans, G., Mickley, L. J., Martin, S. T., Pöschl, U., Andreae, M. O., and Coe, H.: Enhanced aerosol particle growth sustained by high continental chlorine emission in India, Nat. Geosci., 14, 77–84, https://doi.org/10.1038/s41561-020-00677-x, 2021.

Hersbach, H., Bell, B., Berrisford, P., Hirahara, S., Horányi, A., Muñoz-Sabater, J., Nicolas, J., Peubey, C., Radu, R., Schepers, D., Simmons, A., Soci, C., Abdalla, S., Abellan, X., Balsamo, G., Bechtold, P., Biavati, G., Bidlot, J., Bonavita, M., De Chiara, G., Dahlgren, P., Dee, D., Diamantakis, M., Dragani, R., Flemming, J., Forbes, R., Fuentes, M., Geer, A., Haimberger, L., Healy, S., Hogan, R. J., Hólm, E., Janisková, M., Keeley, S., Laloyaux, P., Lopez, P., Lupu, C., Radnoti, G., De Rosnay, P., Rozum, I., Vamborg, F., Villaume, S., and Thépaut, J.: The ERA5 global reanalysis, Q. J. R. Meteorol. Soc., 146, 1999–2049, https://doi.org/10.1002/qj.3803, 2020.

Hu, L., Millet, D. B., Baasandorj, M., Griffis, T. J., Turner, P., Helmig, D., Curtis, A. J., and Hueber, J.: Isoprene emissions and impacts over an ecological transition region in the U.S. Upper Midwest inferred from tall tower measurements, J. Geophys. Res. Atmos., 120, 3553–3571, https://doi.org/10.1002/2014JD022732, 2015.

Ibald-Mulli, A., Wichmann, H.-E., Kreyling, W., and Peters, A.: Epidemiological Evidence on Health Effects of Ultrafine Particles, J. Aerosol Med., 15, 189–201, https://doi.org/10.1089/089426802320282310, 2002.

Jung, J. G., Pandis, S. N., and Adams, P. J.: Evaluation of Nucleation Theories in a Sulfur-Rich Environment, Aerosol Sci. Technol., 42, 495–504, https://doi.org/10.1080/02786820802187085, 2008.

https://doi.org/10.5194/egusphere-2026-4244
Preprint. Discussion started: 31 July 2026

790 Kanawade, V. P., Shika, S., Pöhlker, C., Rose, D., Suman, M. N. S., Gadhavi, H., Kumar, A., Nagendra,
791 S. M. S., Ravikrishna, R., Yu, H., Sahu, L. K., Jayaraman, A., Andreae, M. O., Pöschl, U., and Gunthe,
792 S. S.: Infrequent occurrence of new particle formation at a semi-rural location, Gadanki, in tropical
793 Southern India, Atmos. Environ., 94, 264–273, https://doi.org/10.1016/j.atmosenv.2014.05.046, 2014a.

794 Kanawade, V. P., Tripathi, S. N., Siingh, D., Gautam, A. S., Srivastava, A. K., Kamra, A. K., Soni, V.
795 K., and Sethi, V.: Observations of new particle formation at two distinct Indian subcontinental urban
796 locations, Atmos. Environ., 96, 370–379, https://doi.org/10.1016/j.atmosenv.2014.08.001, 2014b.

797 Kanawade, V. P., Sebastian, M., Hooda, R. K., and Hyvärinen, A.-P.: Atmospheric new particle
798 formation in India: Current understanding and knowledge gaps, Atmos. Environ., 270, 118894,
799 https://doi.org/10.1016/j.atmosenv.2021.118894, 2022.

800 Kerminen, V.-M., Chen, X., Vakkari, V., Petäjä, T., Kulmala, M., and Bianchi, F.: Atmospheric new
801 particle formation and growth: review of field observations, Environ. Res. Lett., 13, 103003,
802 https://doi.org/10.1088/1748-9326/aadf3c, 2018.

803 Kirkby, J., Curtius, J., Almeida, J., Dunne, E., Duplissy, J., Ehrhart, S., Franchin, A., Gagné, S., Ickes,
804 L., Kürten, A., Kupc, A., Metzger, A., Riccobono, F., Rondo, L., Schobesberger, S., Tsagkogeorgas,
805 G., Wimmer, D., Amorim, A., Bianchi, F., Breitenlechner, M., David, A., Dommen, J., Downard, A.,
806 Ehn, M., Flagan, R. C., Haider, S., Hansel, A., Hauser, D., Jud, W., Junninen, H., Kreissl, F., Kvashin,
807 A., Laaksonen, A., Lehtipalo, K., Lima, J., Lovejoy, E. R., Makhmutov, V., Mathot, S., Mikkilä, J.,
808 Minginette, P., Mogo, S., Nieminen, T., Onnela, A., Pereira, P., Petäjä, T., Schnitzhofer, R., Seinfeld,
809 J. H., Sipilä, M., Stozhkov, Y., Stratmann, F., Tomé, A., Vanhanen, J., Viisanen, Y., Vrtala, A., Wagner,
810 P. E., Walther, H., Weingartner, E., Wex, H., Winkler, P. M., Carslaw, K. S., Worsnop, D. R.,
811 Baltensperger, U., and Kulmala, M.: Role of sulphuric acid, ammonia and galactic cosmic rays in
812 atmospheric aerosol nucleation, Nature, 476, 429–433, https://doi.org/10.1038/nature10343, 2011.

813 Komppula, M., Lihavainen, H., Hyvärinen, A. -P., Kerminen, V. -M., Panwar, T. S., Sharma, V. P., and
814 Viisanen, Y.: Physical properties of aerosol particles at a Himalayan background site in India, J.
815 Geophys. Res. Atmos., 114, 2008JD011007, https://doi.org/10.1029/2008JD011007, 2009.

816 Kulmala, M.: Importance of New Particle Formation for Climate and Air Quality, ACS EST Air, 2,
817 710–712, https://doi.org/10.1021/acsestair.5c00095, 2025.

818 Kulmala, M., Maso, M. D., Mäkela, J. M., Pirjola, L., Väkevä, M., Aalto, P., Miikkulainen, P., Hämeri,
819 K., and O'dowd, C. D.: On the formation, growth and composition of nucleation mode particles, Tellus
820 B Chem. Phys. Meteorol., 53, 479, https://doi.org/10.3402/tellusb.v53i4.16622, 2001.

821 Kulmala, M., Vehkamäki, H., Petäjä, T., Dal Maso, M., Lauri, A., Kerminen, V.-M., Birmili, W., and
822 McMurry, P. H.: Formation and growth rates of ultrafine atmospheric particles: a review of
823 observations, J. Aerosol Sci., 35, 143–176, https://doi.org/10.1016/j.jaerosci.2003.10.003, 2004.

824 Kulmala, M., Petäjä, T., Nieminen, T., Sipilä, M., Manninen, H. E., Lehtipalo, K., Dal Maso, M., Aalto,
825 P. P., Junninen, H., Paasonen, P., Riipinen, I., Lehtinen, K. E. J., Laaksonen, A., and Kerminen, V.-M.:
826 Measurement of the nucleation of atmospheric aerosol particles, Nat. Protoc., 7, 1651–1667,
827 https://doi.org/10.1038/nprot.2012.091, 2012.

828 Kulmala, M., Kerminen, V.-M., Petäjä, T., Ding, A. J., and Wang, L.: Atmospheric gas-to-particle
829 conversion: why NPF events are observed in megacities?, Faraday Discuss., 200, 271–288,
830 https://doi.org/10.1039/C6FD00257A, 2017.

831 Kupc, A., Williamson, C. J., Hodshire, A. L., Kazil, J., Ray, E., Bui, T. P., Dollner, M., Froyd, K. D.,
832 McKain, K., Rollins, A., Schill, G. P., Thames, A., Weinzierl, B. B., Pierce, J. R., and Brock, C. A.:
833 The potential role of organics in new particle formation and initial growth in the remote tropical upper

https://doi.org/10.5194/egusphere-2026-4244
Preprint. Discussion started: 31 July 2026

troposphere, Atmos. Chem. Phys., 20, 15037–15060, https://doi.org/10.5194/acp-20-15037-2020, 2020.

Kürten, A., Jokinen, T., Simon, M., Sipilä, M., Sarnela, N., Junninen, H., Adamov, A., Almeida, J., Amorim, A., Bianchi, F., Breitenlechner, M., Dommen, J., Donahue, N. M., Duplissy, J., Ehrhart, S., Flagan, R. C., Franchin, A., Hakala, J., Hansel, A., Heinritzi, M., Hutterli, M., Kangasluoma, J., Kirkby, J., Laaksonen, A., Lehtipalo, K., Leiminger, M., Makhmutov, V., Mathot, S., Onnela, A., Petäjä, T., Praplan, A. P., Riccobono, F., Rissanen, M. P., Rondo, L., Schobesberger, S., Seinfeld, J. H., Steiner, G., Tomé, A., Tröstl, J., Winkler, P. M., Williamson, C., Wimmer, D., Ye, P., Baltensperger, U., Carslaw, K. S., Kulmala, M., Worsnop, D. R., and Curtius, J.: Neutral molecular cluster formation of sulfuric acid–dimethylamine observed in real time under atmospheric conditions, Proc. Natl. Acad. Sci., 111, 15019–15024, https://doi.org/10.1073/pnas.1404853111, 2014.

Lee, S., Gordon, H., Yu, H., Lehtipalo, K., Haley, R., Li, Y., and Zhang, R.: New Particle Formation in the Atmosphere: From Molecular Clusters to Global Climate, J. Geophys. Res. Atmos., 124, 7098–7146, https://doi.org/10.1029/2018JD029356, 2019.

Lehtipalo, K., Yan, C., Dada, L., Bianchi, F., Xiao, M., Wagner, R., Stolzenburg, D., Ahonen, L. R., Amorim, A., Baccarini, A., Bauer, P. S., Baumgartner, B., Bergen, A., Bernhammer, A.-K., Breitenlechner, M., Brilke, S., Buchholz, A., Mazon, S. B., Chen, D., Chen, X., Dias, A., Dommen, J., Draper, D. C., Duplissy, J., Ehn, M., Finkenzeller, H., Fischer, L., Frege, C., Fuchs, C., Garmash, O., Gordon, H., Hakala, J., He, X., Heikkinen, L., Heinritzi, M., Helm, J. C., Hofbauer, V., Hoyle, C. R., Jokinen, T., Kangasluoma, J., Kerminen, V.-M., Kim, C., Kirkby, J., Kontkanen, J., Kürten, A., Lawler, M. J., Mai, H., Mathot, S., Mauldin, R. L., Molteni, U., Nichman, L., Nie, W., Nieminen, T., Ojdanic, A., Onnela, A., Passananti, M., Petäjä, T., Piel, F., Pospisilova, V., Quéléver, L. L. J., Rissanen, M. P., Rose, C., Sarnela, N., Schallhart, S., Schuchmann, S., Sengupta, K., Simon, M., Sipilä, M., Tauber, C., Tomé, A., Tröstl, J., Väisänen, O., Vogel, A. L., Volkamer, R., Wagner, A. C., Wang, M., Weitz, L., Wimmer, D., Ye, P., Ylisirniö, A., Zha, Q., Carslaw, K. S., Curtius, J., Donahue, N. M., Flagan, R. C., Hansel, A., Riipinen, I., Virtanen, A., Winkler, P. M., Baltensperger, U., Kulmala, M., and Worsnop, D. R.: Multicomponent new particle formation from sulfuric acid, ammonia, and biogenic vapors, Sci. Adv., 4, eaau5363, https://doi.org/10.1126/sciadv.aau5363, 2018.

Merikanto, J., Spracklen, D. V., Mann, G. W., Pickering, S. J., and Carslaw, K. S.: Impact of nucleation on global CCN, Atmos. Chem. Phys., 9, 8601–8616, https://doi.org/10.5194/acp-9-8601-2009, 2009.

Middlebrook, A. M., Bahreini, R., Jimenez, J. L., and Canagaratna, M. R.: Evaluation of Composition-Dependent Collection Efficiencies for the Aerodyne Aerosol Mass Spectrometer using Field Data, Aerosol Sci. Technol., 46, 258–271, https://doi.org/10.1080/02786826.2011.620041, 2012.

Mikkonen, S., Romakkaniemi, S., Smith, J. N., Korhonen, H., Petäjä, T., Plass-Duelmer, C., Boy, M., McMurry, P. H., Lehtinen, K. E. J., Joutsensaari, J., Hamed, A., Mauldin Iii, R. L., Birmili, W., Spindler, G., Arnold, F., Kulmala, M., and Laaksonen, A.: A statistical proxy for sulphuric acid concentration, Atmos. Chem. Phys., 11, 11319–11334, https://doi.org/10.5194/acp-11-11319-2011, 2011.

Mishra, S., Tripathi, S. N., Kanawade, V. P., Haslett, S. L., Dada, L., Ciarelli, G., Kumar, V., Singh, A., Bhattu, D., Rastogi, N., Daellenbach, K. R., Ganguly, D., Gargava, P., Slowik, J. G., Kulmala, M., Mohr, C., El-Haddad, I., and Prevot, A. S. H.: Rapid night-time nanoparticle growth in Delhi driven by biomass-burning emissions, Nat. Geosci. 2023 163, 16, 224–230, https://doi.org/10.1038/s41561-023-01138-x, 2023.

Molteni, U., Bianchi, F., Klein, F., El Haddad, I., Frege, C., Rossi, M. J., Dommen, J., and Baltensperger, U.: Formation of highly oxygenated organic molecules from aromatic compounds, Atmos. Chem. Phys., 18, 1909–1921, https://doi.org/10.5194/acp-18-1909-2018, 2018.

https://doi.org/10.5194/egusphere-2026-4244
Preprint. Discussion started: 31 July 2026

Mönkkönen, P., Koponen, I. K., Lehtinen, K. E. J., Hämeri, K., Uma, R., and Kulmala, M.: Measurements in a highly polluted Asian mega city: observations of aerosol number size distribution, modal parameters and nucleation events, Atmos. Chem. Phys., 5, 57–66, https://doi.org/10.5194/acp-5-57-2005, 2005.

Monks, P. S., Granier, C., Fuzzi, S., Stohl, A., Williams, M. L., Akimoto, H., Amann, M., Baklanov, A., Baltensperger, U., Bey, I., Blake, N., Blake, R. S., Carslaw, K., Cooper, O. R., Dentener, F., Fowler, D., Fragkou, E., Frost, G. J., Generoso, S., Ginoux, P., Grewe, V., Guenther, A., Hansson, H. C., Henne, S., Hjorth, J., Hofzumahaus, A., Huntrieser, H., Isaksen, I. S. A., Jenkin, M. E., Kaiser, J., Kanakidou, M., Klimont, Z., Kulmala, M., Laj, P., Lawrence, M. G., Lee, J. D., Liousse, C., Maione, M., McFiggans, G., Metzger, A., Mieville, A., Moussiopoulos, N., Orlando, J. J., O'Dowd, C. D., Palmer, P. I., Parrish, D. D., Petzold, A., Platt, U., Pöschl, U., Prévôt, A. S. H., Reeves, C. E., Reimann, S., Rudich, Y., Sellegri, K., Steinbrecher, R., Simpson, D., Ten Brink, H., Theloke, J., Van Der Werf, G. R., Vautard, R., Vestreng, V., Vlachokostas, Ch., and Von Glasow, R.: Atmospheric composition change – global and regional air quality, Atmos. Environ., 43, 5268–5350, https://doi.org/10.1016/j.atmosenv.2009.08.021, 2009.

Ng, N. L., Kroll, J. H., Chan, A. W. H., Chhabra, P. S., Flagan, R. C., and Seinfeld, J. H.: Secondary organic aerosol formation from *m* -xylene, toluene, and benzene, Atmos. Chem. Phys., 7, 3909–3922, https://doi.org/10.5194/acp-7-3909-2007, 2007.

Ng, N. L., Herndon, S. C., Trimborn, A., Canagaratna, M. R., Croteau, P. L., Onasch, T. B., Sueper, D., Worsnop, D. R., Zhang, Q., Sun, Y. L., and Jayne, J. T.: An Aerosol Chemical Speciation Monitor (ACSM) for Routine Monitoring of the Composition and Mass Concentrations of Ambient Aerosol, Aerosol Sci. Technol., 45, 780–794, https://doi.org/10.1080/02786826.2011.560211, 2011.

Nieminen, T., Kerminen, V.-M., Petäjä, T., Aalto, P. P., Arshinov, M., Asmi, E., Baltensperger, U., Beddows, D. C. S., Beukes, J. P., Collins, D., Ding, A., Harrison, R. M., Henzing, B., Hooda, R., Hu, M., Hõrrak, U., Kivekäs, N., Komsaare, K., Krejci, R., Kristensson, A., Laakso, L., Laaksonen, A., Leaitch, W. R., Lihavainen, H., Mihalopoulos, N., Németh, Z., Nie, W., O'Dowd, C., Salma, I., Sellegri, K., Svenningsson, B., Swietlicki, E., Tunved, P., Ulevicius, V., Vakkari, V., Vana, M., Wiedensohler, A., Wu, Z., Virtanen, A., and Kulmala, M.: Global analysis of continental boundary layer new particle formation based on long-term measurements, Atmos. Chem. Phys., 18, 14737–14756, https://doi.org/10.5194/acp-18-14737-2018, 2018.

Norris, G., Duvall, R., Brown, S., and Bai, S.: EPA Positive Matrix Factorization (PMF) 5.0 Fundamentals and User Guide, U.S. Environmental Protection Agency, Washington, DC, 2014.

Nursanto, F. R., Meinen, R., Holzinger, R., Krol, M. C., Liu, X., Dusek, U., Henzing, B., and Fry, J. L.: What chemical species are responsible for new particle formation and growth in the Netherlands? A hybrid positive matrix factorization (PMF) analysis using aerosol composition (ACSM) and size (SMPS), Atmos. Chem. Phys., 23, 10015–10034, https://doi.org/10.5194/acp-23-10015-2023, 2023.

O'Dowd, C. D., Hämeri, K., Mäkelä, J., Väkeva, M., Aalto, P., De Leeuw, G., Kunz, G. J., Becker, E., Hansson, H., Allen, A. G., Harrison, R. M., Berresheim, H., Kleefeld, C., Geever, M., Jennings, S. G., and Kulmala, M.: Coastal new particle formation: Environmental conditions and aerosol physicochemical characteristics during nucleation bursts, J. Geophys. Res. Atmos., 107, https://doi.org/10.1029/2000JD000206, 2002.

Paatero, P.: The Multilinear Engine—A Table-Driven, Least Squares Program for Solving Multilinear Problems, Including the *n* -Way Parallel Factor Analysis Model, J. Comput. Graph. Stat., 8, 854–888, https://doi.org/10.1080/10618600.1999.10474853, 1999.

https://doi.org/10.5194/egusphere-2026-4244
Preprint. Discussion started: 31 July 2026

Paatero, P. and Tapper, U.: Positive matrix factorization: A non-negative factor model with optimal utilization of error estimates of data values, Environmetrics, 5, 111–126, https://doi.org/10.1002/env.3170050203, 1994.

Pöschl, U.: Atmospheric Aerosols: Composition, Transformation, Climate and Health Effects, Angew. Chem. Int. Ed., 44, 7520–7540, https://doi.org/10.1002/anie.200501122, 2005.

Riccobono, F., Schobesberger, S., Scott, C. E., Dommen, J., Ortega, I. K., Rondo, L., Almeida, J., Amorim, A., Bianchi, F., Breitenlechner, M., David, A., Downard, A., Dunne, E. M., Duplissy, J., Ehrhart, S., Flagan, R. C., Franchin, A., Hansel, A., Junninen, H., Kajos, M., Keskinen, H., Kupc, A., Kürten, A., Kvashin, A. N., Laaksonen, A., Lehtipalo, K., Makhmutov, V., Mathot, S., Nieminen, T., Onnela, A., Petäjä, T., Praplan, A. P., Santos, F. D., Schallhart, S., Seinfeld, J. H., Sipilä, M., Spracklen, D. V., Stozhkov, Y., Stratmann, F., Tomé, A., Tsagkogeorgas, G., Vaattovaara, P., Viisanen, Y., Vrtala, A., Wagner, P. E., Weingartner, E., Wex, H., Wimmer, D., Carslaw, K. S., Curtius, J., Donahue, N. M., Kirkby, J., Kulmala, M., Worsnop, D. R., and Baltensperger, U.: Oxidation Products of Biogenic Emissions Contribute to Nucleation of Atmospheric Particles, Science, 344, 717–721, https://doi.org/10.1126/science.1243527, 2014.

Sahu, L. K., Yadav, R., and Pal, D.: Source identification of VOCs at an urban site of western India: Effect of marathon events and anthropogenic emissions, J. Geophys. Res. Atmos., 121, 2416–2433, https://doi.org/10.1002/2015JD024454, 2016.

Sandradewi, J., Prévôt, A. S. H., Szidat, S., Perron, N., Alfarra, M. R., Lanz, V. A., Weingartner, E., and Baltensperger, U.: Using Aerosol Light Absorption Measurements for the Quantitative Determination of Wood Burning and Traffic Emission Contributions to Particulate Matter, Environ. Sci. Technol., 42, 3316–3323, https://doi.org/10.1021/es702253m, 2008.

Schraufnagel, D. E.: The health effects of ultrafine particles, Exp. Mol. Med., 52, 311–317, https://doi.org/10.1038/s12276-020-0403-3, 2020.

Sebastian, M., Kanawade, V. P., Soni, V. K., Asmi, E., Westervelt, Daniel. M., Vakkari, V., Hyvärinen, A.-P., Pierce, J. R., and Hooda, R. K.: New Particle Formation and Growth to Climate-Relevant Aerosols at a Background Remote Site in the Western Himalaya, J. Geophys. Res. Atmos., 126, https://doi.org/10.1029/2020JD033267, 2021.

Sebastian, M., Kompalli, S. K., Kumar, V. A., Jose, S., Babu, S. S., Pandithurai, G., Singh, S., Hooda, R. K., Soni, V. K., Pierce, J. R., Vakkari, V., Asmi, E., Westervelt, D. M., Hyvärinen, A.-P., and Kanawade, V. P.: Observations of particle number size distributions and new particle formation in six Indian locations, Atmos. Chem. Phys., 22, 4491–4508, https://doi.org/10.5194/acp-22-4491-2022, 2022.

Seinfeld, J. H.: Atmospheric Chemistry and Physics: From Air Pollution to Climate Change, 1st ed., John Wiley & Sons, Incorporated, Newark, 1 pp., 2016.

Sekimoto, K., Li, S.-M., Yuan, B., Koss, A., Coggon, M., Warneke, C., and De Gouw, J.: Calculation of the sensitivity of proton-transfer-reaction mass spectrometry (PTR-MS) for organic trace gases using molecular properties, Int. J. Mass Spectrom., 421, 71–94, https://doi.org/10.1016/j.ijms.2017.04.006, 2017.

Shang, D., Hu, M., Tang, L., Fang, X., Chen, S., Zeng, L., Guo, S., Zhang, Y., and Wu, Z.: New Particle Formation Occurrence in the Urban Atmosphere of Beijing During 2013–2020, J. Geophys. Res. Atmos., 128, e2022JD038334, https://doi.org/10.1029/2022JD038334, 2023.

Simon, L., Favez, O., Petit, J.-E., Canonaco, F., Slowik, J. G., Marchand, C., and Gros, V.: Source apportionment of organic gaseous and particulate compounds using a combined positive matrix

https://doi.org/10.5194/egusphere-2026-4244
Preprint. Discussion started: 31 July 2026

factorization approach in summer (2020) in the Paris region (France), Atmos. Environ., 354, 121269, https://doi.org/10.1016/j.atmosenv.2025.121269, 2025.

Singh, A., Raj, S. S., Panda, U., Kommula, S. M., Jose, C., Liu, T., Huang, S., Swain, B., Pöhlker, M. L., Reyes-Villegas, E., Ojha, N., Vaishya, A., Bigi, A., Ravikrishna, R., Zhu, Q., Shi, L., Allen, J., Martin, S. T., McFiggans, G., Andreae, M. O., Pöschl, U., Coe, H., Bianchi, F., Su, H., Kanawade, V. P., Liu, P., and Gunthe, S. S.: Rapid growth and high cloud-forming potential of anthropogenic sulfate aerosol in a thermal power plant plume during COVID lockdown in India, Npj Clim. Atmos. Sci., 6, 109, https://doi.org/10.1038/s41612-023-00430-2, 2023.

Singh, A., Swain, B., Sebastian, M., Tripathi, S. N., Pöhlker, M., Allan, J., McFiggans, G., Pöschl, U., Su, H., Martin, S. T., Andreae, M. O., Ravikrishna, R., Cheng, Y., Coe, H., Liu, P., and Gunthe, S. S.: Anthropogenic Emissions in Coastal India Strongly Influence New Particle Formation and Cloud Condensation Nuclei Activity, ACS EST Air, 2, 1972–1986, https://doi.org/10.1021/acsestair.5c00180, 2025a.

Singh, K., Gautam, A. S., Jeni Victor, N., Kumar, S., Potdar, S. S., Komsaare, K., and Siingh, D.: Characteristics of new particle formation events at high-altitude location of Western Himalayan Region, Tehri Garhwal, India, Atmos. Res., 315, 107903, https://doi.org/10.1016/j.atmosres.2024.107903, 2025b.

Sipilä, M., Berndt, T., Petäjä, T., Brus, D., Vanhanen, J., Stratmann, F., Patokoski, J., Mauldin, R. L., Hyvärinen, A.-P., Lihavainen, H., and Kulmala, M.: The Role of Sulfuric Acid in Atmospheric Nucleation, Science, 327, 1243–1246, https://doi.org/10.1126/science.1180315, 2010.

Stein, A. F., Draxler, R. R., Rolph, G. D., Stunder, B. J. B., Cohen, M. D., and Ngan, F.: NOAA's HYSPLIT Atmospheric Transport and Dispersion Modeling System, Bull. Am. Meteorol. Soc., 96, 2059–2077, https://doi.org/10.1175/BAMS-D-14-00110.1, 2015.

Sun, J., Hermann, M., Weinhold, K., Merkel, M., Birmili, W., Yang, Y., Tuch, T., Flentje, H., Briel, B., Ries, L., Couret, C., Elsasser, M., Sohmer, R., Wirtz, K., Meinhardt, F., Schütze, M., Bath, O., Hellack, B., Kerminen, V.-M., Kulmala, M., Ma, N., and Wiedensohler, A.: Measurement report: Contribution of atmospheric new particle formation to ultrafine particle concentration, cloud condensation nuclei, and radiative forcing – results from 5-year observations in central Europe, Atmos. Chem. Phys., 24, 10667–10687, https://doi.org/10.5194/acp-24-10667-2024, 2024.

Tang, L., Feng, Z., Shang, D., Zeng, L., Wu, Z., Wang, H., Chen, S., Li, X., Zeng, L., Hu, J., and Hu, M.: Ongoing uncoordinated anthropogenic emission abatement promotes atmospheric new particle growth in a Chinese megacity, Nat. Commun., 16, 6720, https://doi.org/10.1038/s41467-025-62011-6, 2025.

Tiszenkel, L., Flynn, J. H., Dodero, A., and Lee, S.-H.: Sulfuric acid, base, and low-volatility organics contribute to aerosol nucleation in urban Houston, Commun. Earth Environ., 6, 364, https://doi.org/10.1038/s43247-025-02310-4, 2025.

Tripathi, N., Sahu, L. K., Wang, L., Vats, P., Soni, M., Kumar, P., Satish, R. V., Bhattu, D., Sahu, R., Patel, K., Rai, P., Kumar, V., Rastogi, N., Ojha, N., Tiwari, S., Ganguly, D., Slowik, J., Prévôt, A. S. H., and Tripathi, S. N.: Characteristics of VOC Composition at Urban and Suburban Sites of New Delhi, India in Winter, J. Geophys. Res. Atmos., 127, e2021JD035342, https://doi.org/10.1029/2021JD035342, 2022.

Tröstl, J., Chuang, W. K., Gordon, H., Heinritzi, M., Yan, C., Molteni, U., Ahlm, L., Frege, C., Bianchi, F., Wagner, R., Simon, M., Lehtipalo, K., Williamson, C., Craven, J. S., Duplissy, J., Adamov, A., Almeida, J., Bernhammer, A.-K., Breitenlechner, M., Brilke, S., Dias, A., Ehrhart, S., Flagan, R. C., Franchin, A., Fuchs, C., Guida, R., Gysel, M., Hansel, A., Hoyle, C. R., Jokinen, T., Junninen, H.,

https://doi.org/10.5194/egusphere-2026-4244
Preprint. Discussion started: 31 July 2026

1013 Kangasluoma, J., Keskinen, H., Kim, J., Krapf, M., Kürten, A., Laaksonen, A., Lawler, M., Leiminger,
1014 M., Mathot, S., Möhler, O., Nieminen, T., Onnela, A., Petäjä, T., Piel, F. M., Miettinen, P., Rissanen,
1015 M. P., Rondo, L., Sarnela, N., Schobesberger, S., Sengupta, K., Sipilä, M., Smith, J. N., Steiner, G.,
1016 Tomè, A., Virtanen, A., Wagner, A. C., Weingartner, E., Wimmer, D., Winkler, P. M., Ye, P., Carslaw,
1017 K. S., Curtius, J., Dommen, J., Kirkby, J., Kulmala, M., Riipinen, I., Worsnop, D. R., Donahue, N. M.,
1018 and Baltensperger, U.: The role of low-volatility organic compounds in initial particle growth in the
1019 atmosphere, Nature, 533, 527–531, https://doi.org/10.1038/nature18271, 2016.

1020 Wang, L., Slowik, J. G., Tripathi, N., Bhattu, D., Rai, P., Kumar, V., Vats, P., Satish, R., Baltensperger,
1021 U., Ganguly, D., Rastogi, N., Sahu, L. K., Tripathi, S. N., and Prévôt, A. S. H.: Source characterization
1022 of volatile organic compounds measured by proton-transfer-reaction time-of-flight mass spectrometers
1023 in Delhi, India, Atmos. Chem. Phys., 20, 9753–9770, https://doi.org/10.5194/acp-20-9753-2020, 2020.

1024 Warneke, C., De Gouw, J. A., Edwards, P. M., Holloway, J. S., Gilman, J. B., Kuster, W. C., Graus,
1025 M., Atlas, E., Blake, D., Gentner, D. R., Goldstein, A. H., Harley, R. A., Alvarez, S., Rappenglueck,
1026 B., Trainer, M., and Parrish, D. D.: Photochemical aging of volatile organic compounds in the Los
1027 Angeles basin: Weekday-weekend effect, J. Geophys. Res. Atmos., 118, 5018–5028,
1028 https://doi.org/10.1002/jgrd.50423, 2013.

1029 India Population 2026: https://worldpopulationreview.com/countries/india, last access: 6 April 2026.

1030 Yang, C., Brean, J., Xu, W., Xu, L., Huang, W., Fan, X., Bianchi, F., Du, W., Lin, Z., Li, L., Chen, G.,
1031 Zhang, Y., Cai, R., Chen, Y., Li, M., and Chen, J.: Anthropogenic Oxygenated Organic Molecules
1032 Dominate New Particle Growth in Moderate-Pollution Urban China, Environ. Sci. Technol., 60, 6364–
1033 6377, https://doi.org/10.1021/acs.est.5c11555, 2026.

1034 Young, L.-H., Lee, S.-H., Kanawade, V. P., Hsiao, T.-C., Lee, Y. L., Hwang, B.-F., Liou, Y.-J., Hsu,
1035 H.-T., and Tsai, P.-J.: New particle growth and shrinkage observed in subtropical environments, Atmos.
1036 Chem. Phys., 13, 547–564, https://doi.org/10.5194/acp-13-547-2013, 2013.

1037 Yu, H., Ortega, J., Smith, J. N., Guenther, A. B., Kanawade, V. P., You, Y., Liu, Y., Hosman, K., Karl,
1038 T., Seco, R., Geron, C., Pallardy, S. G., Gu, L., Mikkilä, J., and Lee, S.-H.: New Particle Formation and
1039 Growth in an Isoprene-Dominated Ozark Forest: From Sub-5 nm to CCN-Active Sizes, Aerosol Sci.
1040 Technol., 48, 1285–1298, https://doi.org/10.1080/02786826.2014.984801, 2014.

1041 Zhou, L., Hopke, P. K., Stanier, C. O., Pandis, S. N., Ondov, J. M., and Pancras, J. P.: Investigation of
1042 the relationship between chemical composition and size distribution of airborne particles by partial least
1043 squares and positive matrix factorization, J. Geophys. Res. Atmos., 110, 2004JD005050,
1044 https://doi.org/10.1029/2004JD005050, 2005.

1045